Review

Lead-Free Double Perovskites: A Review of the Structural, Optoelectronic, Mechanical, and Thermoelectric Properties Derived from First-Principles Calculations, and Materials Design Applicable for Pedagogical Purposes

David O. Obada [1,2,3,4,*], Shittu B. Akinpelu [5,*], Simeon A. Abolade [1], Emmanuel Okafor [6], Aniekan M. Ukpong [2,7], Syam Kumar R [1,5] and Akinlolu Akande [1,5,*]

[1] Mathematical Modelling and Intelligent Systems for Health and Environment (MISHE) Research Group, School of Science, Atlantic Technological University, F91 YW50 Sligo, Ireland; simeon.abolade@research.atu.ie (S.A.A.); syam.kumar@atu.ie (S.K.R.)
[2] Theoretical and Computational Condensed Matter and Materials Physics Group (TCCMMP), School of Chemistry and Physics, University of KwaZulu-Natal, Pietermaritzburg 3201, South Africa; ukponga@ukzn.ac.za
[3] Multifunctional Materials Laboratory, Department of Mechanical Engineering, Ahmadu Bello University, Zaria 810222, Nigeria
[4] Africa Centre of Excellence on New Pedagogies in Engineering Education (ACENPEE), Ahmadu Bello University, Zaria 810222, Nigeria
[5] Modelling & Computation for Health And Society (MOCHAS), Atlantic Technological University, F91 YW50 Sligo, Ireland
[6] SDAIA-KFUPM Joint Research Center for Artificial Intelligence, King Fahd University of Petroleum and Minerals, Dhahran 31261, Saudi Arabia; emmanuel.okafor@kfupm.edu.sa
[7] National Institute for Theoretical and Computational Sciences (NITheCS), Pietermaritzburg 3201, South Africa
[*] Correspondence: david.obada@atu.ie (D.O.O.); babatunde.akinpelu@research.atu.ie (S.B.A.); akinlolu.akande@atu.ie (A.A.)

Abstract: Metal halide perovskite materials have shown significant advancements in their application as light absorbers in perovskite solar cells, with power conversion efficiencies reaching 27%. However, lead-based perovskites pose a concern due to their toxicity and stability issues in moisture, UV radiation, and heat. This has led to a pressing need to explore substitute materials that do not contain lead but maintain the remarkable characteristics of lead-based perovskites. This review article focuses on halide double perovskites characterised by the $A_2B'B''X_6$ composition, highlighting their structural, optical, thermoelectric, and mechanical capabilities. Additionally, the review evaluates several materials databases to investigate materials suitable for high-throughput first-principles calculations integrated inside density functional theory. The review aims to identify novel perovskite materials, offer a thorough evaluation of the potential benefits and drawbacks associated with this class of materials, and, from the pedagogical standpoint, discover effective instructional frameworks.

Keywords: double perovskites; power conversion efficiency; lead-free materials; light absorbers; perovskite solar cells; metal halide perovskites

1. Introduction

A significant increase in the demand for energy over the years has resulted in the high consumption of fossil fuels. This has contributed significantly to environmental pollution and caused global warming. To combat this energy crisis, renewable energy power sources are necessary [1]. Renewable energy is an energy source that can be replenished, freely produced, and is non-exhaustible. Examples include solar, wind, biomass, wood, geothermal, and tidal, among many others. Recently, there has been rapid usage and dependency on these sources of energy because they are environmentally friendly and

almost limitless. Solar energy as one of these sources of renewable energy; it converts radiation energy from the sun into useful heat and electrical energy via solar photovoltaic (PV) and solar thermal collectors [2]. Silicon solar cells have proven to be the ideal solar cell material. This is due to their high efficiency, reliability, and low cost, and they account for more than half of the photovoltaic energy market. Silicon wafer solar cells have exhibited a few detrimental problems when subjected to space radiation hardness [3,4]. However, silicon solar cells rely heavily on the weather and their installation costs are quite high. Therefore, there is a persistent effort to find alternatives to traditional photovoltaic materials that can be made with cheap, easy, and eco-friendly processes. As a result, there is an ongoing interest in using PV materials created using low-cost, simple, and environmentally responsible technologies [5]. Perovskite materials hold significant importance in the realm of renewable and clean energy due to their exceptional optoelectronic capabilities.

Perovskite solar cells (PSCs) employ perovskite materials as the substrate for capturing photons or light. These materials have demonstrated notable characteristics, including distinct and adjustable bandgaps, significant absorption in the visible spectrum, and elevated carrier mobilities [6]. Over the last decade, these materials have been studied and investigated in energy applications such as photocatalysts [7], (PV) [8], luminescent materials [9], and thermoelectric materials [10]. PSCs that have certified efficiencies that exceed 25% have n-i-p structures, as shown in Figure 1. These structures can be categorised into mesoporous and regular types, with the difference being that the former collects the carriers generated in the perovskite layer [11]. Typically, the perovskite layers sandwiched between the hole and electron transport materials (HTM and ETM) consist of an absorber layer (for instance $CH_3NH_3PbX_3$). When subjected to illumination, the perovskite absorber initiates the production of unbound charge carriers by generating an electron and a hole within the n-type and p-type materials responsible for transporting carriers. The movement of electrons occurs within the mesoporous film and external circuit, facilitating their arrival at the cathode. Simultaneously, the hole-transporting material (HTM) aids in the reversion of oxidised perovskite to its original state and assists in its return to the ground state. Indium tin oxide (ITO) is frequently employed as a transparent conducting oxide (TCO) due to its notable combination of electrical conductivity and optical transparency. There are gaps between these different architectures (Figure 1), particularly the regular and inverted devices in terms of their efficiencies; this has been described in the review on PSCs conducted by Liu et al. [10]. However, before zooming into the core content of this review, a major highlight that is worth noting from the study reported in [10] emphasised the remarkable properties of an inverted p-i-n structure (Figure 1c), which is characterised by intrinsically stable electron charge transport layers and stable metal counter electrodes that have good stability, low hysteresis, and efficiency that is competitive with any other device structure. This makes this class of PSC a promising architecture for the future [12,13].

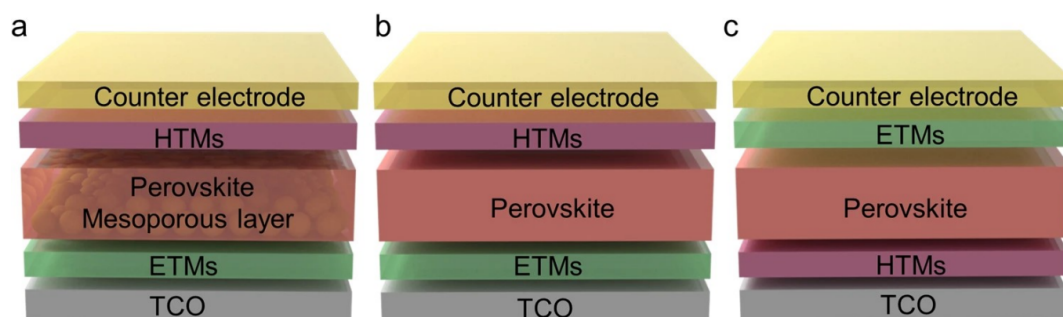**Figure 1.** Structures of PSCs. (**a**) Structure based on perovskite mesoporous layer. (**b**) n–i–p structure (regular). (**c**) p–i–n structure (inverted). Reproduced with permission from [10]. Copyright Springer Nature 2023.

So, if this device architecture will be useful for the PSCs of the future, it is important to review the progress of inverted PSCs. Liu et al. [10] reviewed the progress of research on

the efficiency of inverted PSCs, as shown in Figure 2. The first discovery of the first inverted perovskite solar cell (PSC) was documented in 2013 and demonstrated an efficiency of 3.9% [14]. Two years later, an inverted PSC was reported with a record power conversion efficiency (PCE) of 15% and that showed excellent light stability for over 1000 h, triggering an upsurge in research on improving the efficiency of inverted PSCs [15]. In 2020, the certified PCE of inverted PSCs hit 22% for the first time after years of research [16]. The certified PCE of inverted PSCs has surpassed 23%, 24%, and 25% in recent years [17,18]. The progress made in this study provides comprehensive evidence that inverted PSCs offer numerous advantages in the fabrication of highly efficient modules, hence exhibiting more potential for industrial-scale production.
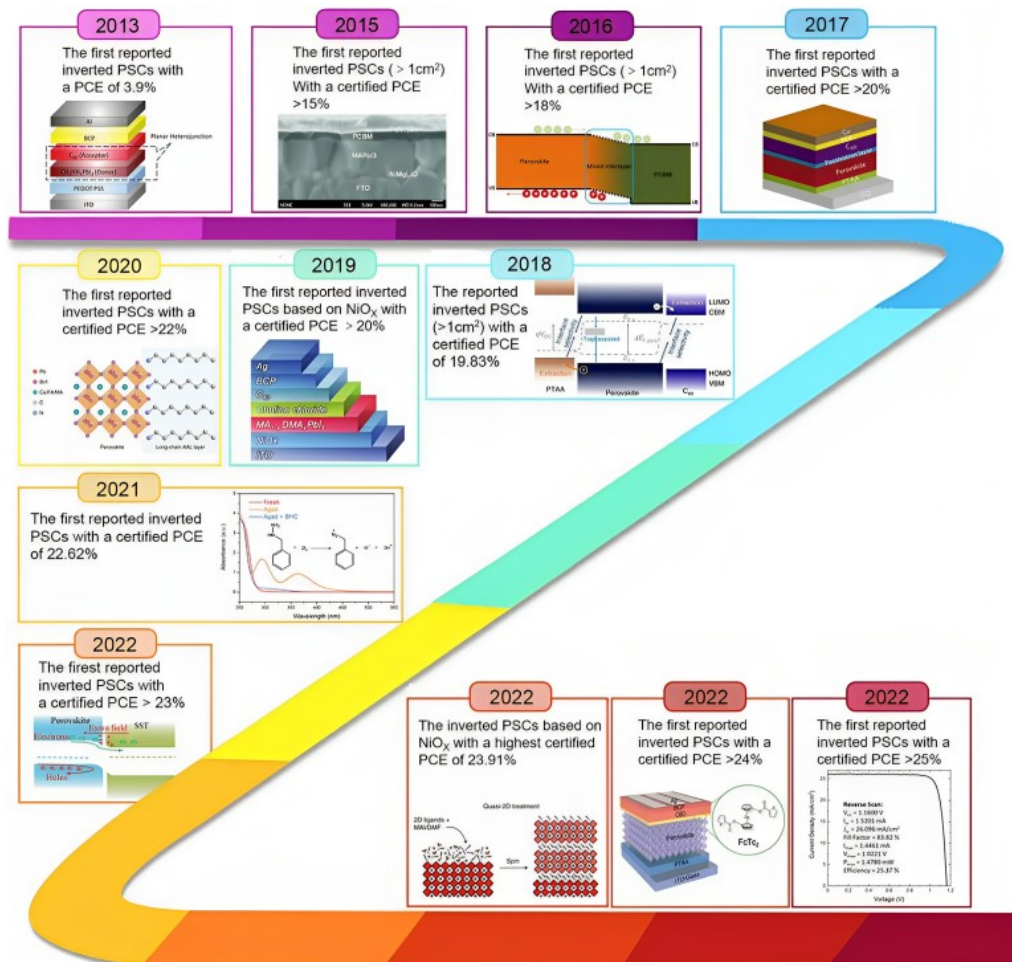
Figure 2. The progress of the efficiencies of inverted PSCs. Reproduced with permission from [10]. Copyright Springer Nature 2023.

The most optimal absorber materials investigated for perovskite solar cells are composed of semiconducting lead halide perovskites with an ABX_3 crystal structure. A represents a monovalent cation that can be either organic or inorganic. B, on the other hand, represents a divalent metal cation with a charge of Pb^{2+}. Lastly, X denotes a counter ion belonging to the halide group. The utilisation of mixed ion methods in photovoltaic systems has the potential to enhance their performance by enabling tuneable features. However, limitations to commercialisation include lead toxicity and bioavailability, water solubility, and chemical instability under ambient conditions [19]. Therefore, it has become essential to find non-toxic and environmentally friendly perovskite materials suitable for solar cell applications. In general, to achieve a pollution- and toxic-free environment, other monovalent and trivalent elements are typically used in place of the hazardous Pb [20–22].

One simple method to replace Pb is to do this with elements that are from the same group (group IV) in the periodic table such as tin (Sn) and germanium (Ge) [23,24]. However, solar cell devices that use Sn and Ge show lower power conversion efficiencies compared with their Pb-based counterparts [25]. Furthermore, Sn and Ge are characterised by the oxidation from their +2 state to +4 state because of their high-energy 5 s and 4 s orbitals. This results in a quick degradation of the perovskite material that does not favour long-term applications [26]. Another option to obtain a Pb-free perovskite while maintaining the structure of the perovskite compound is to replace two Pb^{2+} cations with a pair of non-toxic heterovalent metal cations with oxidations states of +1 and +3. These variants are referred to as "double perovskites" and have a formula of $A_2B(I)^+B(III)^{3+}X_6$ (Figure 3). In the structure of a halide double perovskite, the B^+X_6 and $B^{3+}X_6$ octahedra are alternately arranged so that each B^+ and B^{3+} cation is surrounded by six $B^{3+}X_6$ and B^+X_6 octahedra, respectively. The A cation resides in the cubic octahedral cavity formed by eight octahedra (four pairs of B^+- and B^{3+}-centred octahedra) [27].
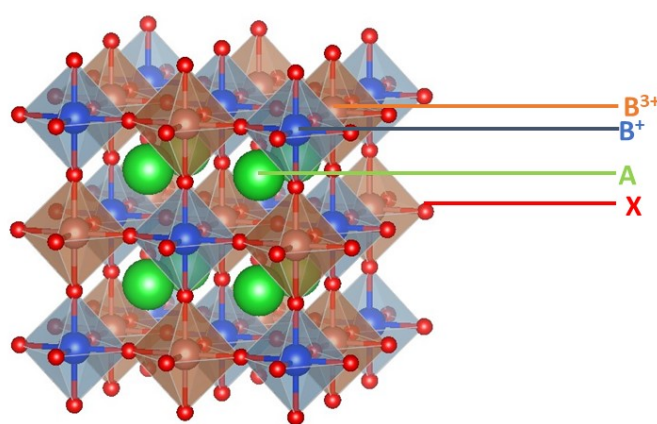

Figure 3. Crystal structure of ideal $A_2B(I)^+B(III)^{3+}X_6$ halide double perovskites.

This variant of double perovskite stands out for their exceptional stability and tuneable physical properties due to changes in the makeup of the A, B^+, B^{3+}, and X-sites. If the two heterovalent metal cations are to be replaced with a single tetravalent metal cation, then that leaves one vacancy site and the general formula becomes $A_2B(IV)^{3+}X_6$ to maintain charge neutrality. This type of double perovskite is referred to as the vacancy-ordered type. The first Pb-free double perovskite is $Cs_2AgBiBr_6$, with efficiency calculated to be 8% [4]. This opened up the possibility of other promising candidates such as $Cs_2InSbCl_6$ and $Rb_2CuInCl_6$ with higher PCE values and suitable bandgaps compared with their organic counterparts [28,29].

Some experimental work on double perovskites includes the work of Wei et al. [30], who synthesised a hybrid double perovskite $(MA)_2KBiCl_6$. This system was identified and showcased notable resemblances to the extensively investigated lead halide perovskites, i.e., $(MA)PbX_3$. Deng et al. [31] synthesised $(MA)_2TlBiBr_6$, and the authors demonstrated in their study that the application of density functional theory (DFT) screening to hybrid double perovskite materials, namely $(MA)_2BIBiX_6$, where BI represents K, Cu, Ag, or Tl and X represents Cl, Br, or I, indicates the likelihood of these systems possessing band gaps comparable with those observed in the $MAPbX_3$ lead compounds, particularly when BI is Cu, Ag, or Tl. Based on these observations, the compound $(MA)_2TlBiBr_6$, which shares the same number of electrons as $MAPbBr_3$, was produced and determined to possess a band gap of approximately 2.0 eV. Volonakis et al. [32] synthesised $Cs_2InAgCl_6$ (where X represents either Cl or Br) and its band gap properties were investigated, revealing that it demonstrates band gaps within the visible spectrum. Nevertheless, it should be noted that the band gaps exhibited by these compounds were of an indirect nature, hence rendering them less than optimal for use in thin-film photovoltaic systems. Subsequently, a novel category of halide double perovskites was suggested by the authors, whereby the B^{3+} and

B^+ cations are represented by In^{3+} and Ag+, respectively. According to their first-principles calculations, it was determined that the hypothetical compounds Cs_2InAgX_6 (X = Cl, Br, or I) are expected to have straight band gaps spanning from the visible (I) to the ultraviolet (Cl) range. Based on the assumptions, the authors endeavoured to synthesise $Cs_2InAgCl_6$ and $Cs_2InAgBr_6$ compounds. As a result of their efforts, they successfully synthesised the hitherto undiscovered double perovskite compound $Cs_2InAgCl_6$. The utilisation of X-ray diffraction analysis resulted in the determination of a double perovskite structure exhibiting the space group Fm-3m. The determined band gap of the compound was 3.3 eV, and it exhibited photosensitivity, undergoing a reversible colour change from white to orange when exposed to ultraviolet (UV) light.

Double perovskites have opened the way for many different combinations, some of which have been investigated using theoretical techniques and experiments [33]. The theoretical and computational efforts have been enhanced using established databases that are applicable for pedagogical purposes. Materials databases store crystallographic structures and properties of materials studied in materials science and engineering. They are developed to find appropriate data from accumulated knowledge. Crystallographic databases, such as the Inorganic Crystal Structure Database, Crystallography Open Database, Cambridge Structural Database, Automated-FLOW for Materials Discovery Library (AFLOWLIB), Materials Project, and American Mineralogist Crystal Structure Database, are popular for atomic structure, point and space group, and density information. The Materials Project (MP) is a high-throughput materials database utilizing first-principles DFT calculations that is part of the materials genome initiative. The MP database, for instance, has significantly supported academics, researchers, etc., in incorporating materials databases into their curriculum to provide diverse information and aid education/research. It is therefore important to investigate these databases as teaching aids to advance the exploration of new compounds suitable for several industrial applications.

Therefore, the main goal of this review is to present snapshots of the materials' properties such as the structural, optoelectronic, and thermoelectric properties of double perovskites from the theoretical standpoint. These theoretical simulations, in addition to the exploration of databases for materials discovery, provide a logical way to establish potential candidates from the many combinations of Pb-free double perovskites.

In what follows (Sections 2–5), we present a review of the properties of this class of materials from a theoretical standpoint, with emphasis on reports and calculations from first principles using DFT. In Section 6, a review of a few materials databases to explore materials applicable in high-throughput first-principles calculations embedded in DFT is presented together with the potential of incorporating several materials databases for teaching and learning. Lastly, the challenges, opportunities, and future directions of Pb-free double perovskites are highlighted.

2. Structural and Electronics Properties

The general chemical formula for double perovskite materials is $A_2B(I)^+B(III)^{3+}X_6$, where A and B^+/B^{3+} are cations and X represents anions. Due to their prospective applications in optoelectronic devices, such as solar cells and light-emitting diodes, as well as in catalysts and sensors, halide double perovskite materials are of particular interest. The majority of halide double perovskites crystallise with a cubic crystal structure Fm-3m and a lattice parameter of 10–12 Å [34]. Halide double perovskites are composed of alternating B^+- and B^{3+}-centred octahedra of B^+ and B^{3+} arranged in a 3D framework known as rock salt order [35]. The halide double perovskites exhibit a structural arrangement that closely mimics that of oxide double perovskites, such as Sr_2FeMoO_6. These oxide double perovskites are renowned for their intriguing characteristics, including ferroelectricity, ferromagnetism, and superconductivity [36]. The crystal structure of halide double perovskites has a significant impact on their properties.

The Goldschmidt rule has been employed over a certain period to ascertain the structural stability of hybrid perovskites that combine organic and inorganic components. Com-

putational screening and experimental validation, such as material synthesis or crystallinity, are commonly used to discover perovskite with possible elements. The investigation of the design of double perovskites involves the application of the Goldschmidt rule to achieve a stable lattice structure, resulting in the development of multiple perovskite compounds that are Pb free. Essentially, there are two parameters necessary to analyse the possibility to form a perovskite structure, the tolerance factor (τ) and the octahedral factor (μ) [37]. The closer the value of τ is to unity, the closer the perovskite is to a cubic structure. As reported in many studies, τ should be $0.875 \leq \tau < 1.107$ and μ should be $0.414 \leq \mu < 0.592$ [38–40] for a cubic structure to be stable. Figure 4 shows a summary of the octahedral (μ) and tolerance (τ) factors of some Pb-free double perovskites and inorganic halide perovskites. Double perovskites with τ values less than 0.85 may not be able to maintain cubic structures [41]. The slight variation of τ for halide double perovskites ensures that cation substitution is robust without affecting the pristine crystal lattice and allows for a more convenient way for designing materials than organic–inorganic halide perovskites.
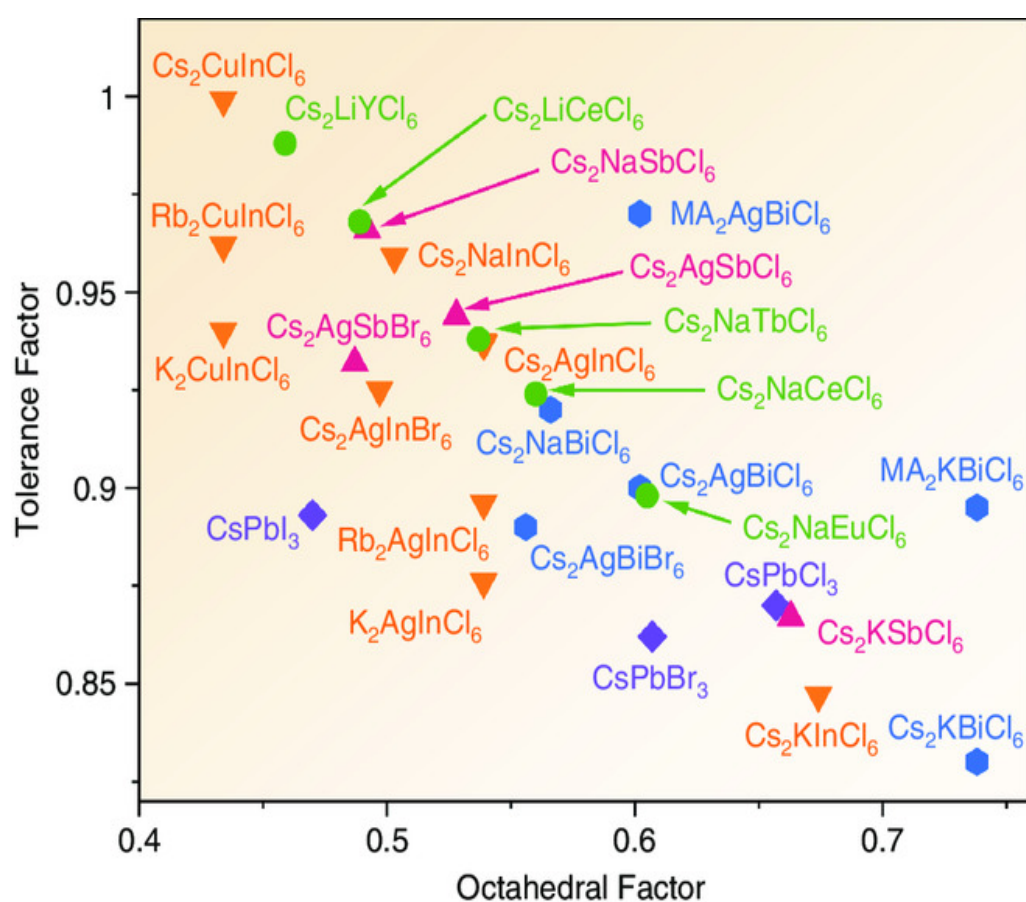
Figure 4. A summary of octahedral factor (μ) and tolerance factor (τ) of Pb-free double perovskites [42]. Reproduced with permission from [42]. Copyright, John Wiley and Sons, 2020.

It is important to review a few studies on the structural properties of Pb-free double perovskites from first-principles calculations and link some properties of the systems to the structural information obtained. Mahmood et al. [43] studied the structural properties of cubic Cs_2GeCl_6 and Cs_2GeBr_6 and concluded that they have the space group of Fm-3m with the lattice constants $a_0 = 10.61$ Å and 11.36 Å, respectively, and the increasing lattice constant ascribed to the replacement of Cl with Br atoms. This is because the atomic radii increase from 1.75 Å (Cl) to 1.85 Å (Br), leading to an increase in the interatomic distance and a decrease in density. This has potential implications for the mechanical properties of the system. Iqbal et al. [44] probed the structural properties of cubic $Rb_2AlInCl_6$, $Rb_2AlInBr_6$, and Rb_2AlInI_6 and reported their implications on the bulk modulus of the system. It

was observed that the lattice constants obtained were inversely proportional to the bulk modulus because the applied stresses can change the volume and a rise in the ionic radius can enhance the lattice constants. In the work reported by Mahmood [45], a vacancy-ordered double perovskite Rb_2PdX_6 (X = Cl, Br) was investigated in the cubic phase Fm-3m. It was observed that, structurally, all the PdX_6 in the system was separated by 12-fold coordination that reduces the bond length. An increase in the lattice constants were noticed when the anions were replaced.

In terms of the stability of the structures of Pb-free double perovskites based on tolerance and octahedral factors, Kibbou et al. [46] studied the $Cs_2InGaCl_6$ perovskite and reported excellent crystal stability in addition to high cubic symmetry because of the tolerance factor of 0.92 and the octahedral factor of 0.53, which aligns with the range stable octahedral factor of the cubic structure (0.44–0.90). In the study by Noor et al. [47], the lattice constants increased from Rb_2ScInI_6 to Cs_2ScInI_6, and this was ascribed to the increase in atomic radii from 2.48 Å (Rb) to 2.65 Å (Cs). An increase in the size of the cations decreased the density of the materials, with a consequent increase in the bulk modulus from 18.85 GPa to 17.95 GPa when Cs was replaced by Rb. In the work conducted by Chrafih et al. [48], it was reported that the structural orientations of the Cs_2AgBiX_6 perovskite consists of an octahedra that was joined via the edges formed by a combination of Ag^+- and Bi^{3+}-centred octahedra, which was noticeable through all three orientations with a consequent rock salt order superstructure. However, it was mentioned that limitations exist for the unalloyed double perovskites in optoelectronic applications because the Cs_2AgBiX_6 (X = Cl, I, and Br) has indirect bandgaps. Therefore, the parity of the dipolar transitions that exists between the band edge states are prohibited and this results in comparatively large optical bandgaps. Kumar et al. [49] also buttressed the point that Cs_2AgBiX_6 compounds are one of the most promising and studied systems that could serve as an alternative to lead halide perovskites. The Cs_2AgBiX_6 (X = Cl, I, and Br) perovskites were cubic with face-centred structures and a space group of Fm-3m. It was reported that as the halides were changed from Cl to I, there was an increase in the ionic radius that led to an increase in the lattice constant and ground state energies and a consequent decrease in the bulk modulus when the derivative pressure remained constant. The structural properties of K_2AgSbX_6 (X = Cl, Br) were reported by Iqbal et al. [50]. The calculated lattice constants increased as the atomic radii of the halides increased. They emphasised that when Br was replaced by Cl, the increase in interatomic separation was evident due to a change in the anionic weight and that this reduced the densities and hardnesses of the solids. They further analysed the stability of the materials' structures using the Goldsmith's tolerance factor (τ) and concluded that the investigated halides were cubic-phase stable.

Talebi et al. [51] reported the structural properties of A_2TiI_6 (A = Cs or NH_4) compounds. They categorised the stability of the perovskite into two aspects, crystallographic stability and thermodynamic stability, which were investigated via the Goldschmidt tolerance factor and the decomposition into competing phases from the energy standpoint, respectively. The calculated tolerance factors for the systems show that the structures are stable. The calculated octahedral factors showed that in the Ti-based perovskite structures where the octahedral factor is lower than 0.414, the titanium cation was noticed not to be in contact with the iodide anions in the octahedra, which typically results in a lower coordination number. Therefore, the octahedron system $[TiI_6]^2$ was slightly not stable. This can be ascribed to the large polarizability of the I anion. In the work conducted by the authors of [52] on the Rb_2NaCoF_6 perovskite, the calculated optimised parameters, such as lattice parameters, equilibrium volume, bulk modulus, and the pressure derivative of the bulk modulus, were in agreement with experimentally calculated values and the calculated formation energy showed that the compound can be easily synthesised.

The performance of photonic devices is significantly influenced by optoelectronic qualities. An increase in the lattice parameters of halide perovskite systems enlarges the bandgap. The bandgap of a semiconductor, for example, is closely related to its crystal structure. The bandgap in halide double perovskites can be modified by adjusting the

composition and crystal structure [21]. In the presence of defects such as vacancies or impurities, halide double perovskites are able to retain their properties due to their high defect tolerance [53]. Consequently, they are intriguing candidates for use in electronic and optoelectronic devices due to their tuneable bandgap, high defect tolerance, and high absorption coefficients [54]. Some halide double perovskites have demonstrated promising solar cell efficiencies; however, challenges remain in terms of stability and long-term performance [55].

Two major families of Cs_2AgBiX_6 and Cs_2AgInX_6 compounds have been widely evaluated; however, their disadvantages, such as long-term stability and indirect band gaps, hinder their use as an active layer for PSCs. Furthermore, most of the Pb double perovskites either theoretically or experimentally have shown to be characterised by indirect bandgaps [56–58]. For instance, the Cs_2AgBiX_6 compounds have indirect bandgaps [59] that have been determined by measurements. $CsAgBiX_6$ showed an indirect bandgap of 1.98 eV. This indirect bandgap was ascribed to the chemical mismatch between the Ag and Bi cations. The DFT calculations suggested that the conduction band minimum (CBM) of Cs_2AgBiX_6 was mainly composed of the Bi-6p/halogen-p antibonding states, whereas the valence band maximum (VBM) was located at the X point, resulting in the indirect bandgap configuration [60]. Comparing this to some experimentally determined bandgaps for Pb-free double perovskites, it can be observed from Figure 5 that the Bi-based double perovskites $Cs_2AgBiBr_6$ and $Cs_2AgBiCl_6$ show a broad distribution of the values of bandgaps. These variations can be attributed to synthesis routes and characterization methods, in addition to the selected models used for the calculations. Therefore, theoretical calculations can bridge the gap with regards to the experimentally observed inconsistencies, thereby widening the scope of the systems that can be designed for efficient light harvesting.
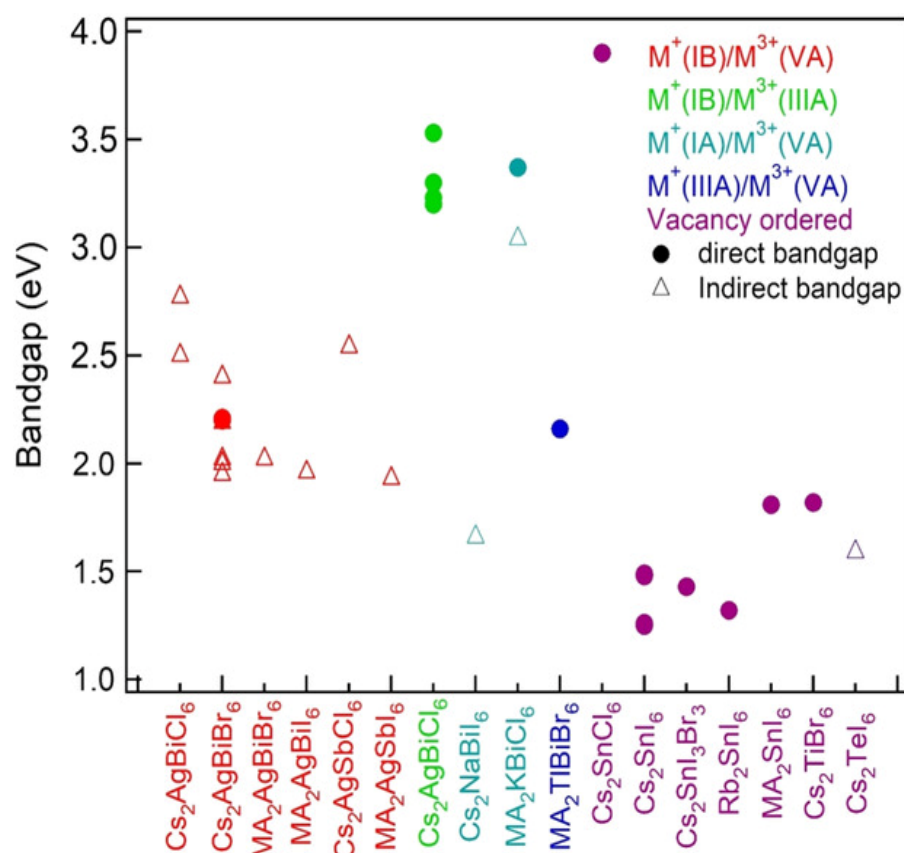

Figure 5. Variation in bandgap values for experimentally derived double perovskites [4]. Reproduced with permission from [4]. Copyright, John Wiley and Sons, 2019.

When predicting the bandgaps of materials theoretically using DFT, two commonly used functionals are the Perdew–Burke–Ernzerhof (PBE) and the Heyd–Scuseria–Ernzerhof (HSE). The accuracy of the HSE functional could be enhanced with a dependence on the fraction of exact exchange included [61]. It is important to continually investigate the variation in bandgaps, as this plays a very important role in the application of PSCs. To improve on the limitations of DFT and hybrid functionals, the single-particle Green's function and the screened Coulomb interaction (GW) approximation have been applied regardless of the high computational resources required. Some studies have attempted to obtain accurate bandgaps using GW approximation [57]. This was conducted by comparing the values of the bandgaps obtained with experimentally derived ones. It was revealed that the electronic states of Ag^+ in $Cs_2AgBiCl_6$ and $Cs_2AgBiBr_6$ double perovskites was a crucial factor in GW calculations. This accuracy in calculations was further investigated by the authors of [61], who compared the calculated results with the more accurate GW calculations and concluded that with the selection of the proper exchange correlation for the HSE calculations, the two calculations (GW and HSE) presented a reasonable agreement. In Figure 6, the calculated electronic band structure of Cs_2AgBiX_6 obtained using DFT calculations using GW is displayed. The large indirect bandgap observed can be detrimental for efficient application as a photovoltaic system. The reduction of large bandgaps can be achieved by incorporating smaller elements from the halogens column, resulting in the attainment of appropriate direct bandgaps, as stated in the literature [62].
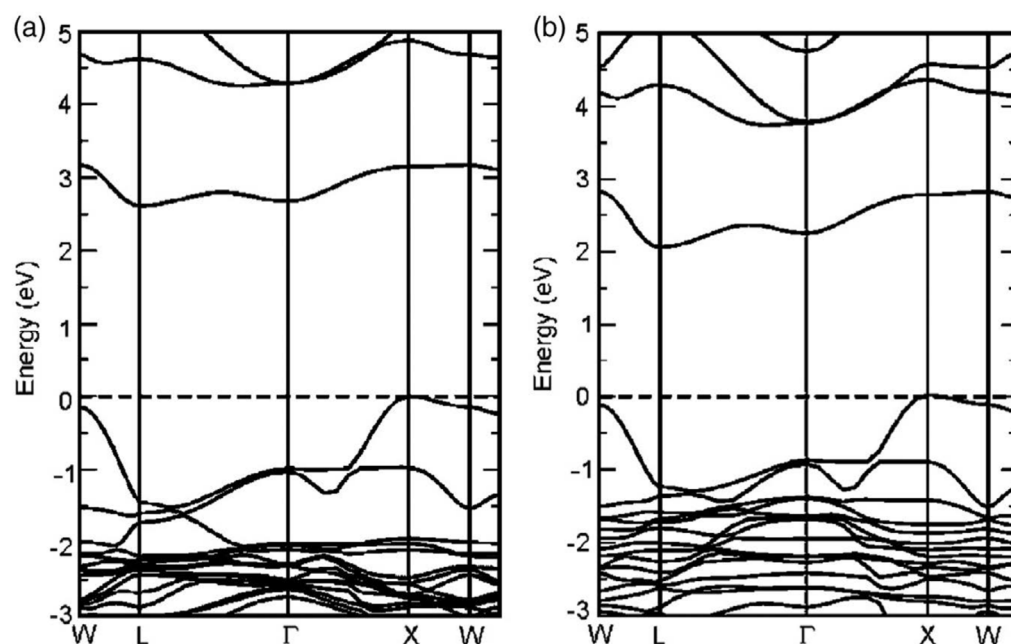
Figure 6. Calculated DFT electronic band structures of (**a**) $Cs_2AgBiCl_6$ and (**b**) $Cs_2AgBiBr_6$. Reproduced with permission from [60]. Copyright, American Chemical Society, 2016.

The relationship between bandgap (electronic properties) and lattice constant (structural properties) in perovskite materials is a complex one, as both properties can be influenced by a variety of factors, including the type and arrangement of atoms in the crystal lattice structure. The bandgap of a material is an essential property that determines its electronic and optical characteristics [63]. This property is determined by the electronic structure of the atoms in the material and their interactions within the crystal lattice [64]. The size and shape of the lattice structure can affect the distance between atoms, which in turn can affect the overlap between electronic orbitals and the formation of electronic bands. Electronic bands refer to the ranges of energies that electrons can occupy, and the bandgap is the energy range that cannot be occupied by electrons. The lattice constant, which corresponds to the distance between adjacent atoms in the crystal lattice, also plays

a significant role in determining the electronic and optical properties of a material. It affects the strength of atomic bonds and the formation of electronic bands. Changes in the lattice constant can alter the electronic structure of a material, which in turn can affect its bandgap [65]. However, the relationship between the lattice constant and the bandgap is not straightforward, and it can vary depending on the specific material and its crystal structure. Understanding the relationship between these two properties is critical for designing and engineering materials with specific electronic and optical properties.

A recent article by Tang and Tang [33] investigated the optoelectronic properties of some double perovskite materials, namely Cs_2AgMX_6 (M = Co, Rh, Ir; X = Cl, Br, I), and observed that the lattice constants of the compounds were between 10 and 11.6 Å. It was observed that a double perovskite with a chlorine atom as the halide has lower lattice parameters and a higher the bandgap. This is due to the decrease in the ionic radius of Co (0.75 Å), Rh (0.68 Å), and Ir (0.625 Å). The trend of the lattice constant and bandgap was also noticed with a double perovskite material with a Br atom as the halide. The bandgaps are relatively lower than those with Cl. Considering the iodine halide, the trend in the ionic radius as we move from cobalt to iridium and iodine plays a significant role in increasing the lattice constant and bandgap as observed in Table 1. It would be worth noting that the overall bandgap of the material is not influenced by the ionic radius of the halides. Chlorine has an ionic radius of 1.81 Å, bromine has an ionic radius of 1.96 Å, and iodine has an ionic radius of 1.33 Å, with the highest bandgaps observed for $Cs_2AgRhCl_6$ (2.418 eV), $Cs_2AgIrBr_6$ (1.96 eV), and Cs_2AgIrI_6 (1.274 eV). However, it would be noted that as we move down the halogen group, the overall bandgap reduces.

Considering the work by Iqbal et al. [50], the optoelectronic and thermoelectric properties of K_2AgSbX_6 (X = Cl, Br) double perovskites were studied using first-principles calculations, and the lattice constants increased with the ionic radius whereas the bandgap decreased with increases in the lattice constant. An increase in the lattice constant caused an increase in the bandgap of the materials as the antimony is replaced with bismuth. In a related study by Maqsood et al. in 2022 [66], the chlorine halide perovskite material was interchanged at the A site with rubidium and caesium in the double perovskite material K_2AgSbX_6 (X = Cl, Br), with gradients observed in the bandgap values. Radja et al. [67] carried out a theoretical calculation on $Cs_2AgFeCl_6$ using a first-principles study. The bandgap (1.18 eV) falls into a good bandgap range for thermoelectric and optoelectronic applications.

In the study by Murtaza et al. [68], the double perovskites $Rb_2TlAgCl_6$ and $Cs_2TlAgCl_6$ were studied. It can be observed that thallium in the composition plays an important role in lowering the bandgap (0.72 eV) and increasing the lattice constant (10.52 Å) compared with $Cs_2AgRhCl_6$, which has a lattice constant of 10.32 Å and bandgap of 2.418 eV [33]. $Rb_2TlAgCl_6$ had a higher bandgap than $Cs_2TlAgCl_6$ because Rb has higher electronegativity than Cs, which resulted in an increase in the energy levels.

In a more recent study by Kattan et al. [69], first-principles and experimental studies were carried out on tuning the bandgap by anion variation of K_2AgInX_6 (X = Cl, Br, I) double perovskites for solar cells and thermoelectric applications. When the halide site was substituted with different halogens, it was observed that as the electronegativity decreased down the halide groups, the lattice constants increased from 10.32 Å (Cl) to 10.86 Å (Br) and 11.79 Å (I), whereas the bandgap reduced as well as and left the least electronegative halogen in the set (iodine) to have a metallic bandgap. In 2021, Shah and Niaz [70] used DFT to investigate Pb-free indium silver-based double perovskites for thermoelectric applications. An increase in the ionic radius caused higher lattice constants and lower bandgaps in $Cs_2InAgCl_6$, $Rb_2InAgCl_6$, and $K_2InAgCl_6$. The lattice constant of $K_2InAgCl_6$ has a percentage difference of about 3% compared with the $K_2AgInCl_6$ reported in the work performed by Kattan et al. [69] due to the fact that a different DFT code and functionals were used.

$Cs_2InBiCl_6$, $Cs_2InBiBr_6$, and Cs_2InBiI_6 were investigated by Aslam et al. in 2021 [71] by using the DFT to estimate their bandgaps and lattice constants. It was observed that

the lower the ionic radius, the lower the bandgap and the larger the lattice constant. $Na_2CuSbCl_6$ and $Na_2CuBiCl_6$ double perovskites were investigated by Al-Qaisi et al. in [72]. The increase in the ionic radius between antimony (0.76 Å) and bismuth (1.03 Å) could be noticed in the increase in the lattice constant and bandgap when exchanging the B^{3+} sites. Hu et al. [73] revealed the electronic and optical properties of $K_2CuBiBr_6$ and $K_2CuBiCl_6$ via first-principles calculations. In this study, it was discovered that the ionic radii of Br and Cl contributed to the increase in the chloride site more than the bromide halide site. Zhao et al. [74] worked on Cs_2NaBX_6 (B = Sb, Bi; X = Cl, Br, I). Bismuth has higher electronegativity than antimony, and this affected the value of the bandgap, as reflected in Table 1, which shows a summary of the structural and electronic properties of the reviewed double perovskite compounds and the functionals used for the DFT calculations.

Table 1. A summary of the structural and electronic properties of the reviewed double perovskite compounds and the functionals used for the DFT calculations. The compounds were arranged based on the atomic number of the element in the A site followed by the same in B, B', and X sites.

S/N	Materials	Lattice Parameter Å	Bandgap (eV)	Bandgap Type	Functionals	Ref.
1	$Na_2ScAgCl_6$	10.19	3.63	direct	PBE	[68]
2	$Na_2CuSbCl_6$	10.29	0.66	indirect	PBE	[72]
3	$Na_2CuBiCl_6$	10.41	0.94	indirect	PBE	[72]
4	$K_2ScAgCl_6$	10.26	3.65	direct	PBE	[68]
5	$K_2CuBiCl_6$	10.47	1.44	indirect	HSE06	[73]
6	$K_2CuBiBr_6$	11.05	1.03	indirect	HSE06	[73]
7	$K_2AgInCl_6$	10.32	2.37	direct	TB-Mbj	[69]
8	$K_2AgInBr_6$	10.86	1.34	direct	TB-Mbj	[69]
9	K_2AgInI_6	11.79	0.00	direct	TB-Mbj	[69]
10	$K_2AgSbCl_6$	10.66	2.30	indirect	mBJ	[50]
11	$K_2AgSbBr_6$	11.22	1.51	indirect	mBJ	[50]
12	K_2AgSbI_6	12.01	0.70	indirect	mBJ	[50]
13	K_2AgBiI_6	12.11	1.21	indirect	mBJ	[75]
14	$K_2InAgCl_6$	10.66	1.12	direct	PBE	[70]
15	Rb_2KScI_6	12.15	2.75	direct	mBJ	[75]
16	$Rb_2InAgCl_6$	10.66	1.11	direct	PBE	[70]
17	$Rb_2TlAgCl_6$	10.45	0.78	direct	TB-Mbj	[76]
18	$Cs_2NaSbCl_6$	10.65	3.13	indirect	PBE	[74]
19	$Cs_2NaSbBr_6$	11.22	2.54	indirect	PBE	[74]
20	Cs_2NaSbI_6	12.06	1.90	direct	PBE	[74]
21	$Cs_2NaBiCl_6$	10.84	3.73	indirect	PBE	[74]
22	$Cs_2NaBiBr_6$	11.36	3.07	indirect	PBE	[74]
23	Cs_2NaBiI_6	12.20	2.23	direct	PBE	[74]
24	Cs_2KScI_6	12.17	2.65	direct	mBJ	[75]
25	$Cs_2AgCrCl_6$	10.17	0.00		HSE06	[33]
26	$Cs_2AgFeCl_6$	10.48	1.18	indirect	mBJ	[67]

Table 1. *Cont.*

S/N	Materials	Lattice Parameter Å	Bandgap (eV)	Bandgap Type	Functionals	Ref.
27	$Cs_2AgCoCl_6$	10.21	2.34	indirect	HSE06	[33]
28	$Cs_2AgCoBr_6$	10.73	1.66	indirect	HSE06	[33]
29	Cs_2AgCoI_6	11.51	0.78	indirect	HSE06	[33]
30	$Cs_2AgRhCl_6$	10.32	2.42	direct	HSE06	[33]
31	$Cs_2AgRhBr_6$	10.83	1.85	indirect	HSE06	[33]
32	Cs_2AgRhI_6	11.59	0.85	indirect	HSE06	[33]
33	$Cs_2AgIrCl_6$	10.35	2.40	direct	HSE06	[33]
34	$Cs_2AgIrBr_6$	10.88	1.96	direct	HSE06	[33]
35	Cs_2AgIrI_6	11.61	1.27	indirect	HSE06	[33]
36	$Cs_2InCoCl_6$	10.47	0.00		HSE06	[33]
37	$Cs_2InAgCl_6$	10.69	1.07	direct	PBE	[70]
38	$Cs_2InBiCl_6$	11.27	1.84	indirect	TB-Mbj	[71]
39	$Cs_2InBiBr_6$	11.71	1.27	indirect	TB-Mbj	[71]
40	Cs_2InBiI_6	12.41	0.65	indirect	TB-Mbj	[71]
41	$Cs_2TlAgCl_6$	10.52	0.74	direct	TB-Mbj	[68]

3. Optical Properties

Optical properties refer to the interaction of light with matter, including the reflection, refraction, absorption, transmission, and emission of light. The optical properties of materials play a critical role in various energy applications, including solar cells, lighting, and displays. Understanding the optical properties of materials can help improve their efficiency and performance in these applications. The Pb-free double perovskites are characterised by direct and indirect bandgaps, which has implications for their optical properties. The halide double perovskites have been reported to have bandgaps that are useful for photovoltaic applications. Although their organic counterparts may be thermally unstable, hybrid halide double perovskites have shown excellent thermal stability [6]. Tang and Tang, 2023 [33], conducted a theoretical study on Cs_2AgMX_6 (M=Co, Rh, Ir; X = Cl, Br, I) perovskites and reiterated that the optical properties of the materials are crucial for their practical applications. The complex dielectric function, which determines the interaction between light and the material, can be expressed as $\varepsilon(\omega) = \varepsilon_1(\omega) + i\varepsilon_2(\omega)$. The real part ($\varepsilon_1$) and imaginary part ($\varepsilon_2$) of the dielectric function can be used to deduce other optical properties. The static real part of the dielectric function ($\varepsilon_1(0)$) increases in the order Cl, Br, and I, and the values for Co and Rh are nearly the same and larger than that for Ir [33]. The refractive index (n) varied between 1.32 and 2.45, indicating that electromagnetic waves would be slowed down by the reaction between electrons. The materials exhibit low reflectivity within the UV-visible-IR region (0–7 eV), indicating that most photons within this energy range are not reflected by the materials. The optical conductivity (σ) values are around one in the 0–6 eV region and increase rapidly to high peaks in the far UV region. The utilisation of light is directly influenced by the light absorption coefficient, and the absorption edges of the curves alter in response to changes in the transition metals and halogens. Among the various perovskite variations that have been investigated, $Cs_2AgCoBr_6$ has been identified as a highly promising candidate for solar energy conversion. This selection is primarily attributed to its favourable alignment with the solar AM1.5 irradiance spectrum and its suitable bandgap.

Probing into more theoretical studies on the optical properties of double perovskites, Iqbal et al. [50] showed the optical properties of K_2AgSbX_6 (X = Cl, Br) compounds by

computing their reflectivity, refractive index, absorption coefficient, optical conductivity, and dielectric constant. The results showed that both compounds had a complete optical absorption propensity in the visible range of the electromagnetic spectrum and are suitable for use in optical and electrical devices. The absorption of $K_2AgSbCl_6$ in the visible region was found to be lower than that of $K_2AgSbBr_6$. Additionally, energy loss was observed in both compounds at certain frequencies, with $K_2AgSbCl_6$ having a higher maximum energy loss compared with $K_2AgSbBr_6$. The study also showed that the maximum reflectivities for the compounds were observed at 3.85 eV and 4.3 eV, respectively. These values show that the optical properties of semiconductors can provide valuable insights into their electronic and vibrational states. In the study conducted by Manzoor et al. [75], they aimed at investigating the optical properties of double perovskites for optoelectronics applications by analysing the material nature through computing the absorption and refractive index. The real and imaginary parts of the dielectric function were calculated using the Kramer–Kronig relation, which describes the transition and absorption in materials by applying photon energy on the material surface. The study found that K_2AgSbI_6 and K_2AgBiI_6 had different bandgaps due to their bond states. The bonding in K_2AgBiI_6 was found to be more covalent, leading to a lower sharing of electrons in solid interaction materials, whereas K_2AgSbI_6 had a narrower bandgap due to the fast transition of electrons from the valence band to the conduction band. Additionally, the study found that at high energy levels, semiconductor materials can behave like metals, which causes the material to demonstrate the plasmatic resonance frequency. The extinction coefficient and absorption coefficient were also analysed, and the static values of the refractive index and dielectric constant confirmed the findings. Maqsood et al. [66] conducted a study on the electronic and optical properties of Rb_2KScI_6 and Cs_2KScI_6 halides with bandgap values of 2.75 eV for Rb_2KScI_6 and 2.65 eV for Cs_2KScI_6. The bandgaps were in the visible region of the electromagnetic spectrum, which made the halides potential candidates for use in solar cell devices. The study also analysed the total density of states (TDOS) and partial density of states (PDOS) of the halides to evaluate their electrical behaviour. The optical properties of Rb_2KScI_6 and Cs_2KScI_6, such as refractive index, reflectivity, extinction coefficient, absorption coefficient, and dielectric constant, were computed. The computed values of these properties showed that the halides exhibited optimal optical properties for use in electronic applications. The study concluded that Rb_2KScI_6 and Cs_2KScI_6 showed potential for use in solar cell devices and other electronic applications.

The article by Murtaza et al. from 2021 [76] discusses the optical properties of two compounds, $Cs_2AgTlCl_6$ and $Rb_2AgTlCl_6$. The real parts of the (ε_1) of $Cs_2AgTlCl_6$ and $Rb_2AgTlCl_6$ both show features of small energy bandgap semiconductors. The static dielectric function of $Cs_2AgTlCl_6$ exhibits a greater value compared with $Rb_2AgTlCl_6$, which is mostly attributed to the narrower bandgap seen in $Cs_2AgTlCl_6$. The increase in photon energy is accompanied by a corresponding increase in ε_1, which attains its peak value within the visible spectrum before declining inside the ultraviolet range. The compound based on Cs exhibits a higher degree of charge polarisation in comparison with the compound based on Rb. The refractive index $n(\omega)$ spectra of the two compounds follow the pattern of ε_1, with different magnitudes due to their relation. The absorption coefficient shows high absorption in the visible range, with the peak value for $Cs_2AgTlCl_6$ being smaller than that for $Rb_2AgTlCl_6$ due to its larger length. The compounds exhibit low optical reflectivity in the visible range and undergo a significant decrease in reflectivity as the wavelength shifts towards the ultraviolet area. The relationship between the loss function and the decrease in reflectivity of the compounds shows a positive connection, whereas the plasmon oscillations reach their maximum intensity in the ultraviolet (UV) region.

In a related study conducted by Kattan et al. [69], the optical properties of K_2AgInX_6 (X = Cl, Br) using parameters such as $\varepsilon(\omega)$, $n(\omega)$, $\alpha(\omega)$, $R(\omega)$, and $L(\omega)$ were discussed. The static values of $\varepsilon_1(\omega)$ are related to bandgaps and increase to peaks at 3.6 eV and 2.5 eV for $K_2AgInCl_6$ and $K_2AgInBr_6$, respectively. The addition of the Br ion shows more dispersion than the Cl ion, indicating the importance of anion variation to enhance optical applications.

The $n(\omega)$ values increased with the incident energy and show that $K_2AgInCl_6$ is suitable for optoelectronic devices in ultraviolet regions, whereas $K_2AgInBr_6$ is important for solar cells in the visible region. The absorption bands fall in the energy range from 3.0 eV to 4.5 eV and from 2.0 eV to 3.5 eV for $K_2AgInCl_6$ and $K_2AgInBr_6$, respectively. The (ω) and $L(\omega)$ values should be at the bare minimum for the best optical materials. The study's findings indicate that $K_2AgInBr_6$ holds greater significance for solar cells in comparison with $K_2AgInCl_6$ due to its reduced energy loss and higher absorption values within the visible region.

In a report by Aldaghfag et al. [68], the optical characteristics of $K_2ScAgCl_6$ and $Na_2ScAgCl_6$ for their potential use in optoelectronic and photovoltaic device applications were discussed. Theoretical calculations using the frequency-dependent complex dielectric function were used to determine various parameters that define the optical response of the materials. The dielectric constant and reflectivity values of both compounds were determined to be rather low within the energy range spanning from zero to the bandgap value. This suggests that both compounds possess transparency to incident photons within this range, making them favourable options to produce lenses operating within this energy range. The process of compound absorption initiates at an energy level of 0 eV and exhibits its initial peak at 4.5 eV for both compounds. The refractive index of the materials was also determined and it was found that the maximum values for the refractive index of $Na_2ScAgCl_6$ and $K_2ScAgCl_6$ were 2.19 and 2.0, respectively, at 4.2 eV. Calculating various optical parameters for Cs_2InBiX_6 compounds (where X is Cl, Br, or I) to determine their potential for optoelectronic applications was conducted by Aslam et al. [71]. The optical parameters studied included the real and imaginary dielectric constant, refractive index, absorption coefficient, optical conductivity, energy loss function, and reflectivity. The study concluded that Cs_2InBiX_6 is appropriate for optical device applications due to its metallic nature in the UV energy range when considering the real part of the dielectric constant and direct bandgap. Thus, the study's findings reveal the potential for practical optoelectronic applications of Cs_2InBiX_6.

A recent study by Hu et al. [73] investigated the optical properties of K_2CuBiX_6 in the photon energy range of 0–8 eV. The complex dielectric function was used to describe the optical response of the material, which can be separated into real and imaginary parts of the dielectric function, $\varepsilon_1(\omega)$ and $\varepsilon_2(\omega)$, respectively. The first peaks of $\varepsilon_1(\omega)$ for K_2CuBiX_6 appeared at 1.79 eV and 2.04 eV, indicating a strong electrical polarization behaviour in the visible light range. The first absorption peaks of K_2CuBiX_6 (X = Br, Cl) were located at 2.65 eV and 2.84 eV, respectively, mainly generated by the transition of Cu-d and Bi-p electrons at VBM to the hybrid orbitals of Bi-p at CBM. The absorption coefficient curves showed that K_2CuBiX_6 has a broad absorption spectrum in the UV-visible wavelength range and that the first characteristic peaks appeared around 400 nm. The findings suggest that K_2CuBiX_6 has great potential in the application of PV and optoelectronic devices due to their strong electrical polarization behaviour and broad absorption spectrum in the visible and near-UV ranges. The study of Zhao et al. [74] aimed to investigate the visible-light harvesting capacity of several double perovskite compounds using DFT. The absorption coefficients of these compounds were calculated and it was found that those with narrow bandgaps, such as Cs_2NaSbI_6, Cs_2NaBiI_6, and $Cs_2NaSbBr_6$, exhibited efficient absorption in the visible range. However, the bandgaps of these compounds were of the indirect type, which impacted the absorption magnitude. A comparison with $CsPbI_3$ (Figure 7), which is predicted to be a direct bandgap semiconductor, showed the difference in absorption. Among the compounds studied, $Cs_2NaBiCl_6$ was the only one experimentally synthesised, but it had a lower absorption range than 320 nm, making it unsuitable for solar cells. However, it could be explored for applications in UV sensors or detectors.
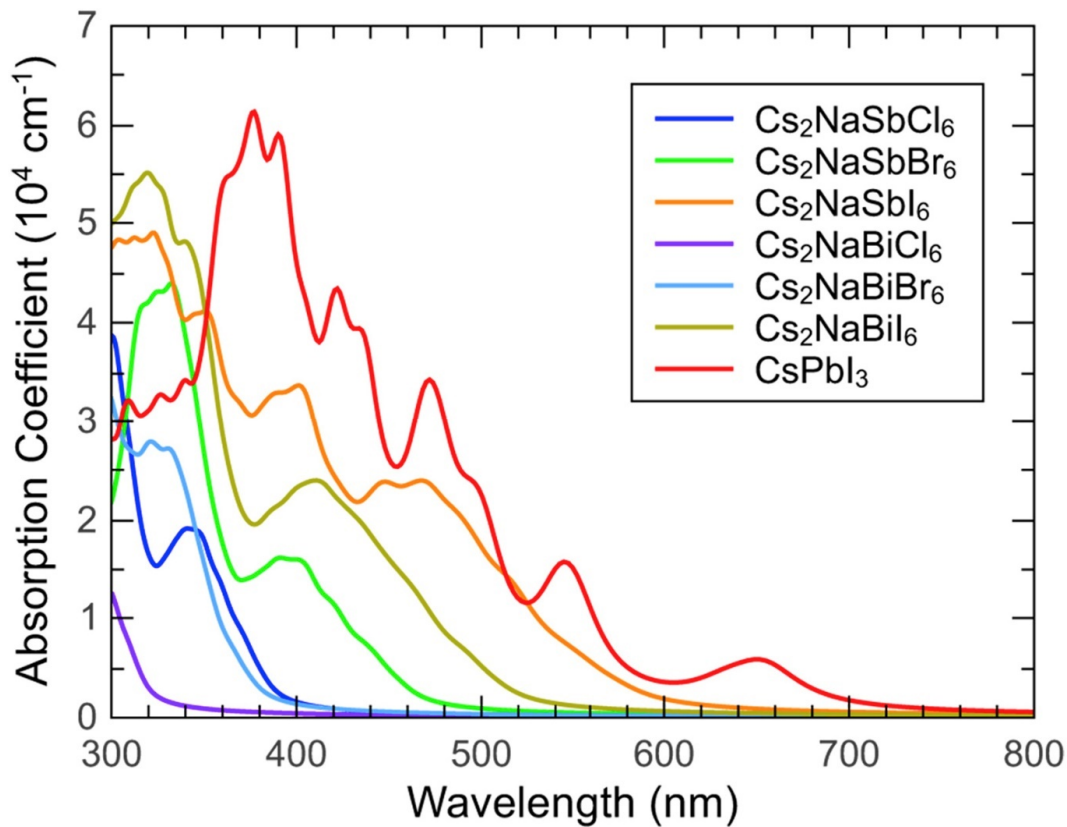
Figure 7. DFT calculated optical properties for double perovskites compounds. Reproduced with permission from [74]. Copyright Elsevier 2018.

4. Thermoelectric Properties

The low thermal conductivity of halide perovskites makes them suitable for thermoelectric applications. Recently, HP-based thermoelectrics have shown significant improvement due to the optimization of relevant parameters. This section focuses on the theoretical progress of enhancing the thermoelectric performance of halide Pb-free double perovskites. The efficiency of thermoelectric materials could be determined through their figure of merit using Equation (1):

$$ZT = \frac{S^2 \sigma T}{K_e + K_l} \tag{1}$$

where S = Seebeck coefficient, T = absolute temperature, σ = electrical conductivity, K_e = electronic thermal conductivity, and K_l = lattice thermal conductivity [77].

Thermoelectric materials with a ZT of approximately unity are effective for thermoelectric applications [78]. This can be achieved with materials exhibiting low thermal conductivity (K) and a high power factor (PF). Despite having extremely low cation activities and high charge mobility in their octahedral structure, these halide double perovskites have mainly been studied for optoelectronic applications.

In the study reported in [77], double perovskites based on $SrTiO_3$ ($Sr_2TiB_9O_6$) were reported to have the potential to be high-temperature thermoelectric materials that were environmentally friendly. Double perovskite materials have been extensively studied due to their various properties, such as ferroelectricity, superconductivity, and halfmetallic behaviour. When different types of B site cations are used, the electrical, magnetic, and thermal properties of the $A_2B_2O_6$ double perovskite structure can be modified. Additionally, these materials have a complex crystal structure that can accommodate multiple cations that can act as phonon scattering centres necessary for low lattice thermal conductivity. Some papers have reported on the thermoelectric properties of double perovskites [79–83],

with a few reports on how important the selection of the elements for the A-site and B-site cations are for optimum thermoelectric performance.

Although the number of experimental investigations on thermoelectric efficiency remains limited, there is a growing interest in exploring the thermoelectric properties of halide perovskites. For instance, Guechi et al. studied the thermoelectric properties of Cs_2AgBiX_6 (X = Cl, Br) using the FP-LAPW approach in combination with the semi-classical Boltzmann transport theory [84]. It was discovered in their findings that these compounds possess a large thermopower Seebeck coefficient that makes them suitable for thermoelectric applications. Additionally, according to the report by Aslam et al., when investigating the thermoelectric features of Cs_2InAgX_6 (X = Cl, Br, I) they observed that the properties of these systems reveal that they are appropriate for thermoelectric applications over a large temperature range 100–800 K [71]. Mumtaz et al. examined the potential ability of K_2AgXI_6 (X = Sb, Bi) for thermoelectric applications. Their results showed that these materials are potential candidates for thermal devices [75]. In addition, Maqsood et al. explored the Rb_2KScI_6 and Cs_2KScI_6 class of double perovskites for thermoelectric applications. The calculated electrical and thermal conductivity ratio analysed in their findings revealed that the materials were observed in the limit of 105, which identifies their suitability for thermoelectric purposes. The value of the figure of merit (ZT) was computed to be around 0.74 for both materials at room temperature and decreases with an increase in temperature [66]. Furthermore, first-principles investigations of Na_2CuMCl_6 (M = Bi, Sb) double perovskites carried out by Al-Qaisi et al. revealed a ZT near to unity due to the semiconducting nature of the materials, indicating the effectiveness of these materials for thermoelectric technology [72]. Therefore, considering that most halide double perovskites have been widely investigated for thermoelectric applications, certain groups making up these compounds are yet to be fully explored, and this can be achieved through a robust computational throughput screening using DFT and machine learning methods, as explained in Section 6 of this review.

5. Mechanical Properties

The mechanical properties of double perovskite compounds have a significant impact on the suitability and overall performance of Pb-free double perovskites for several applications. As reported in Table 2, most of the reported structures are ductile, which makes them suitable for industrial applications. Only Cs_2KScI_6 and Rb_2KScI_6 were calculated to be brittle based on the value of the Pugh and Poisson ratios. The rest of the materials show ductility as they have a Pugh ratio greater than 1.6 [85] and a Poisson ratio greater than 0.3 [86].

The mechanical properties of double perovskite compounds play a significant role in determining the suitability and overall effectiveness of lead-free double perovskites in diverse applications. The investigation of elastic constants is of utmost importance in comprehending the mechanical characteristics of materials and their reaction to external forces. The sources offer valuable insights into the structural, thermomechanical, and chemical characteristics of various materials. The elastic response of a cubic structure is solely determined by the C_{11}, C_{12}, and C_{44} constants, which are derived from the stiffness matrix. C_{11} characterises the material's ability to withstand changes in length resulting from the application of axial stress on the (100) plane in the <100> direction. The C_{12} denotes the intrinsic property of a substance to withstand the alteration caused by the application of axial (longitudinal) stress on the (100) crystallographic plane, along the <010> direction. The material's resistance to deformation resulting from the application of tangential shear stress on the (010) plane in the <001> direction is denoted as C_{44}. The elastic constants of solids establish a connection between the mechanical and dynamic properties, thereby offering crucial insights into the underlying forces at play within a solid. Specifically, they provide insight pertaining to the stability and rigidity of materials.

The overall energy of the system has a greater dependence on volume as compared with strain. In this review, the contribution of volume to the overall energy can be removed

by employing volume conserving strains. The conventional criteria for mechanical stability in cubic crystals are as follows:

$C_{11} - C_{12} > 0$, $C_{11} > 0$, $C_{44} > 0$, $C_{11} + 2C_{12} > 0$, $C_{11} - C_{12}$.

The bulk modulus (B) and shear modulus (G) can be determined by using the elastic constants. Whereas the bulk modulus is the ratio of the tensile stress to tensile strain, the shear modulus is the ratio of the shear stress to shear strain. The ductility or plasticity of a material is positively correlated with a high B/G ratio, whereas a low B/G ratio is indicative of brittleness. The crucial value, denoted as 1.75, serves as the threshold that distinguishes between ductile and brittle materials. Specifically, when the ratio of B to G exceeds 1.75, the material exhibits ductile behaviour, and if the ratio is below this amount, the material demonstrates brittle behaviour. The value of Poisson's ratio (υ) agrees with the ratio of bulk modulus (B) to shear modulus (G), which often characterises ductile materials that have a relatively high Poisson's ratio (υ > 0.26). According to the data presented in Table 2, a significant proportion of the studied structures demonstrate a favourable ductile response, making them highly suitable for a range of industrial applications [85,86].

Table 2. A summary of the reported mechanical properties of some double perovskites. All compounds presented in the Table are mechanically stable.

S/N	Materials	Nature of the Material	Pugh Ratio	Poisson Ratio	Ref.
1	$Na_2CuSbCl_6$	ductile	2.90	0.35	[72]
2	$Na_2CuBiCl_6$	ductile	2.42	0.32	[72]
3	$K_2CuBiCl_6$	ductile	4.04	0.39	[73]
4	$K_2CuBiBr_6$	ductile	2.80	0.34	[73]
5	$K_2AgSbCl_6$	ductile	2.45	0.32	[50]
6	$K_2AgSbBr_6$	ductile	6.69	0.42	[50]
7	Rb_2KScI_6	brittle	1.27	0.19	[66]
8	Cs_2KScCI_6	ductile	2.07	0.29	[87]
9	Cs_2KScBr_6	ductile	2.30	0.31	[87]
10	Cs_2KScI_6	brittle	1.57	0.25	[66]
11	$Cs_2AgFeCl_6$	ductile	2.17	0.30	[67]
12	$Cs_2AgCoCl_6$	ductile	3.41	0.37	[33]
13	$Cs_2AgCoBr_6$	ductile	2.61	0.33	[33]
14	Cs_2AgCoI_6	ductile	2.81	0.34	[33]
15	$Cs_2AgRhCl_6$	ductile	2.80	0.34	[33]
16	$Cs_2AgRhBr_6$	ductile	2.60	0.33	[33]
17	Cs_2AgRhI_6	ductile	2.54	0.33	[33]
18	$Cs_2AgIrCl_6$	ductile	2.84	0.34	[33]
19	$Cs_2AgIrBr_6$	ductile	2.73	0.34	[33]
20	Cs_2AgIrI_6	ductile	3.05	0.35	[33]

6. Design and Discovery of Double Perovskite Materials Using Machine Learning (ML) and Databases to Teach the Concepts

6.1. Machine Learning for Materials Discovery

The applicability of the artificial intelligence approach as a computational tool in discovering and designing novel materials is rapidly evolving within the field of the material research domain. This speedy evolution driven by machine (ML) learning currently opens a blueprint for the development of new materials [88]. The conventional trial-and-error approach predominantly hinges upon the researcher's expertise and intuition,

necessitating substantial investments of time and resources. Nevertheless, the utility of first-principles calculations has played a significant role in expediting the exploration and identification of novel materials to a certain degree [89]. However, the classical and first-principles-based methodologies have inherent constraints in expediting the search process, especially in scenarios involving compounds characterised by intricate molecular configurations. In comparison with ML, first-principles calculations necessitate a greater allocation of computing resources and entail a tedious and higher computational complexity. The investigation of material datasets obtained from experimental studies or first-principles calculations can aid in creating ML models that exhibit the prowess to significantly decrease the duration of the search process involved in the identification of high-performance materials [90,91].

Within the context of exploring machine learning based on training supervised learning for predicting material properties, supervised learning schemes often rely on data preparation and feature engineering (presenting data in a suitable vectorial representation) [92,93]. The resulting features are passed to a learning algorithm by optimizing the weights via computing a weight update rule by estimating the gradient of the predictive error cost function based on the weights. This is based on an end goal to generate optimal weights that would enable effective model generalization and prediction of testing examples of material properties. To further assess model diversity, it is often normal to explore the selection of various models and optimise hyperparameters to enable effective model prediction. The digitisation of material properties can be achieved through data mapping [93] and then harnessed with ML to gain further predictive insights. ML has been extensively utilised to accelerate the discovery of materials and investigate their underlying structural–property relationships, thereby overcoming the conventional experimental and computational approaches via a data-driven approach that can shorten the development cycle of materials [94,95]. An illustration of the general workflow for ML in discovering materials for industrial applications is shown in Figure 8. These include data preparation, feature engineering, model selection, model evaluation, and model application.

The development of ML models often depends on a refined material dataset comprising both dependent and independent variables. Independent variables are frequently referred to as input features or descriptors that represent information about the structure and characteristics of materials. Examples include the chemical composition and atomic or molecular parameters. The dependent variables are the target properties of materials affected by independent variables (also known as target variables). Data quantity and quality are crucial to material discovery using ML [96]. The number of samples needed varies depending on the ML model and general rule of thumb: it is important to pass enough training examples in mini batches to machine learning algorithms to guarantee effective generalization prowess. This stated philosophy is supported by the fact that an algorithm based on artificial neural networks requires many samples [97] to enable it to improve its generalization capability. Data can be obtained from existing open-source code or data repositories (Kaggle, Github, Zenodo, and OSF) or the published literature. Databases encompasses a diverse range of data derived from various sources such as experiments, simulations, and model generations from machine learning. The implementation of data standardization has the potential to enhance ML model accuracy and convergence speed. The outcomes of multiple ML algorithms may exhibit variability depending on whether standardization or scaling techniques are applied or not. It is important to acknowledge that both feature and target variables have the potential to undergo scaling (normalization) [98]. Before creating an ML model, it is vital to ascertain the pivotal elements that are closely associated with the target properties [93]. To ensure effective training and mitigate the risk of overfitting, the data scientist or analyst should make an informed decision about the feature selection and assess the degree of feature correlation. The latter decision can enable suppression of one or more feature that exhibits a strong level of feature correlation (share similarity) and retain features that exhibit moderate or low-level feature correlation. Hence, it is imperative for feature selection to minimise the dimensionality of the input space

while retaining crucial information. To ensure the effectiveness and precision of models, it is essential to exclude redundant features and those with strong self-correlation [99]. To achieve optimal representation of material properties, material features need to satisfy three key criteria: flawless representation of the attributes in question, sensitivity to the desired target properties, and ease of obtainability [100].

The development of ML models has increasingly focused on the creation of predictive models and several studies have employed ML for predicting the properties of double perovskite materials. Shi et al. created an online platform that performs the precise forecasting of the surface area of ABO_3 perovskites [101]. In the year 2016, Pilania et al. introduced a robust machine learning model that relied on elemental descriptors. This model demonstrated a high level of accuracy in predicting the electronic bandgap values of AA'BB'O6 double perovskite materials. The dataset, which comprised approximately 1300 double perovskites, was trained and tested using the statistical learning model known as kernel ridge regression (KRR). The cross-validation of the best model yielded a coefficient of determination and a root mean square error (RMSE = 0.132 eV) in the training phase. On the other hand, in the testing phase, the authors reported an RMSE of 0.360 eV; this result depicts a robust model fitting and excellent generalization capability. The test results demonstrated that there exists a strong agreement with the DFT calculation outcomes. Furthermore, this ML technique has the prowess to be utilised on various materials within a limited chemical space, i.e., those possessing a predetermined crystal structure, to achieve precise predictions of the energy gap [92].
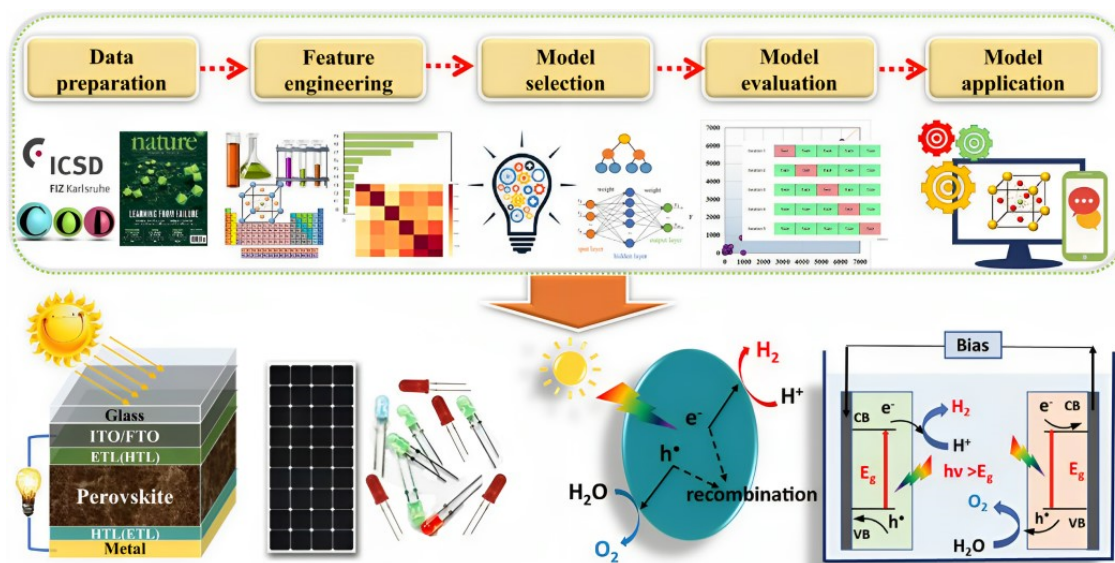

Figure 8. Schematic pipeline of an ML during the prediction of the energy levels in perovskite materials. The process includes data preparation, feature engineering, model selection, model evaluation, and model application. Reproduced with permission from [102]. Copyright Springer Nature 2021.

A hierarchical screening methodology that involves the sequential application of two supervised learning models was employed. The first model was designed for bandgap classification, whereas the second model is intended for bandgap regression. Both models were subject to cross-validation and exhibited predictive capabilities. The classification model was utilised to distinguish materials with wide bandgaps ≥ 0.5 eV or relatively small bandgaps, specifically (<0.5 eV). The second regression model was employed to provide a quantitative estimation of the bandgap value for the wide bandgap compounds. A down-selection process was conducted on a total of 13,589 cubic oxide perovskite compositions. The compositions were chosen based on their predicted ability to be experimentally formed, thermodynamic stability, and possession of a wide bandgap. A specific group of

310 compounds was selected for further investigation because their predicted stability and high confidence level of formation surpassed 90%. Performance metrics were used for systematic analysis and examination of the inter-dependence of model features. Their findings revealed that the quantitative bandgap prediction model established reasonable confidence intervals and the accuracy of their predictions validated that of DFT computations [103]. Furthermore, Junfei et al. predicted the calculated bandgaps of double perovskites using ML. A random forest regression model was used on a training and testing dataset that consisted of 1306 bandgaps. Within the set of 20 physical features considered, it was observed that the bulk modulus, superconductivity temperature, and cation electronegativity displayed the most significant importance scores, which aligns with the principles of the underlying electronic structure in physics. The model also achieved an accuracy of 85.6% and exhibited a root mean square error of 0.64 eV, which is consistent with previous findings. It was stated in their findings that the efficacy of ML regressions can be efficient in evaluating prospective functional materials [104]. Based on the existing literature, it has been observed that ML exhibits significant potential and benefits in the domain of material discovery since it has proven to be effective in uncovering the connections between structural and compositional materials constituents. Despite the existence of certain successful research endeavours, the utilisation of ML in the field of material research remains at an early stage of development. Consequently, a substantial amount of additional effort is required to increase progress within the domain of double perovskite materials.

6.2. Databases to Teach the Concepts of Materials Discovery

Computational materials science and engineering have made significant progress in accelerating the discovery and application of advanced materials using simulation-based design approaches and integrated computational materials engineering (ICME). This review section focuses on data-driven frameworks of ICME, highlighting key aspects, such as principles, databases, and platforms, that can be valuable in teaching computational materials science. Therefore, we present the use of a few materials databases to explore materials for use through high-throughput first-principles calculations embedded in DFT. These provide insights into the structural, electronic, optical, thermoelectric, dynamic mechanical stability, mechanical properties, and molecular dynamics simulations. For context, the utilization of computational methods, such as DFT, plays a paramount role in the discovery and design of new materials [105].

Emerging fields of interest, such as data science and ML, further emphasise the significance of these methods. It is imperative for students, scientists, and researchers, hereafter known as users in materials innovation, to be proficient in both computational methods and physical experimentation as well as have professional skills. An approach would be to ensure that science and engineering students are introduced to simulation projects early on that cover DFT and Python coding to investigate semiconducting materials. These experiences are intended to foster an appreciation for computational methods in comprehending a material's behaviour and properties. Additionally, users can take an introductory Python coding class to establish basic programming skills. In addition, it is possible to use the open-source Quantum Espresso to employ DFT models in calculating the properties of semiconductors. This reinforces their initial forays into first-principles investigations and leads to a more profound understanding of the role of computational materials discovery and design. Multiple databases have been identified for teaching the concepts of computational materials science using DFT, which include the Open Quantum Materials Database (OQMD) [106], the Materials Project [107], the Computational Materials Repository [108], and AFLOWLIB [109,110].

To initiate access to scientific materials from a database, users are advised to commence by navigating to the website of the database and thoroughly engage with the materials repository. Upon successful identification of the target materials, users are advised to proceed by selecting the designated name and subsequently accessing its dedicated page. Next, it is expected that a comprehensive analysis of the given material specifications be

conducted, including essential data such as the molecular formula, crystal lattice, and other characteristics. To obtain the requisite material data, users are presented with a variety of options. The retrieval of fundamental data from the material's page or the systematic access of data can be achieved through the utilization of an application programming interface (API). Users may potentially be presented with the prospect of procuring data files that are correlated with the given material(s). Following the collection of data, users may utilise appropriate tools and software to analyse the acquired data. The manipulation of the compounds' sites (for instance cation and anion sites) can be achieved without compromising the crystal structure or chemical formula, thereby enabling the investigation of alternative elemental compositions. It is imperative for users to duly acknowledge the sources of their data by citing the relevant databases or publications, which ensures the rightful attribution of the data utilised in their research. The systematic procedure outlined herein confers the ability of the users to obtain priceless resources and exploit the information for their scientific endeavours, which enhances their experiential learning outcomes. The computational labs offer cutting-edge methods in materials science, including DFT, phase field modelling, and computational mechanics. Users will develop proficiency in statistical analysis, supervised and unsupervised ML, and data visualization. One project entails reproducing materials data science figures from high-impact papers using free Python packages and the Materials Project API. Additionally, users will gain knowledge about informatics packages such as Pymatgen and Matminer. Furthermore, PRISMS software can be utilised to teach users how to modify and run open-source codes and integrate two different computational methods.

7. Conclusions

The review discusses advancements made by several researchers in enhancing the properties of Pb-free double perovskites through theoretical results on structural, electronic, mechanical, optical, and thermoelectric aspects. In summary, the outcomes of this review article can be listed as follows:

1. Studies suggest that material bandgaps can be altered through metal doping, alloying, or introducing defects. Further research is crucial to understand the relationship between crystal structure, lattice constants, and bandgaps in Pb-free halide double perovskites, which will aid in developing tailored materials for specific electronic and optical applications.
2. Double perovskites display favourable optical absorption for photovoltaic applications. Certain compounds with indirect bandgaps could find use in UV sensors. Additionally, the strong ductility of most of the compounds investigated in this review suits diverse industrial applications such as in catalysis, fuel cells, and electrochemical sensing.
3. Although Pb-free halide double perovskites are extensively studied for thermoelectric purposes, certain groups remain inadequately explored. This review proposes utilizing a robust computational screening approach by employing DFT and machine learning methods to fill these gaps in understanding.
4. ML holds great potential in materials discovery and understanding the relationship between structural, compositional, technical characteristics, and performance. However, its use in material study is still in its early stages and requires further research to improve our understanding.
5. The systematic data extraction techniques discussed in this review allow users to access valuable resources, enhance experiential learning, and develop proficiency in materials science.

Author Contributions: Conceptualization, D.O.O., S.B.A., S.A.A. and A.A.; writing—original draft preparation, D.O.O., S.B.A., S.A.A., A.M.U. and A.A.; writing—review and editing, D.O.O., S.B.A., S.A.A., E.O., A.M.U., S.K.R. and A.A.; supervision, A.M.U. and A.A.; project administration, A.A.; funding acquisition, D.O.O., A.M.U. and A.A. All authors have read and agreed to the published version of the manuscript.

Data Availability Statement: Data sharing is not applicable to this article.

Conflicts of Interest: The authors declare no conflict of interest. The funders had no role in the writing of the manuscript, or in the decision to publish the results.

References

1. Kim, G.-H.; Kim, D.S. Development of Perovskite Solar Cells with >25% Conversion Efficiency. *Joule* **2021**, *5*, 1033–1035. [CrossRef]
2. Dixit, S. Solar Technologies and Their Implementations: A Review. *Mater. Today Proc.* **2020**, *28*, 2137–2148. [CrossRef]
3. Glunz, S.; Preu, R.; Biro, D. Crystalline Silicon Solar Cells: State-of-the-Art and Future Developments. In *Comprehensive Renewable Energy*; Elsevier: Amsterdam, Netherlands, 2012; Volume 1, pp. 353–387, ISBN 978-0-08-087873-7.
4. Kung, P.-K.; Li, M.-H.; Lin, P.-Y.; Jhang, J.-Y.; Pantaler, M.; Lupascu, D.C.; Grancini, G.; Chen, P. Lead-Free Double Perovskites for Perovskite Solar Cells. *Solar RRL* **2020**, *4*, 1900306. [CrossRef]
5. Jebakumar, J.P.A.; Moni, D.J.; Gracia, D.; Shallet, M.D. Design and Simulation of Inorganic Perovskite Solar Cell. *Appl. Nanosci.* **2022**, *12*, 1507–1518. [CrossRef]
6. Meyer, E.; Mutukwa, D.; Zingwe, N.; Taziwa, R. Lead-Free Halide Double Perovskites: A Review of the Structural, Optical, and Stability Properties as Well as Their Viability to Replace Lead Halide Perovskites. *Metals* **2018**, *8*, 667. [CrossRef]
7. Li, X.; Zhao, H.; Liang, J.; Luo, Y.; Chen, G.; Shi, X.; Lu, S.; Gao, S.; Hu, J.; Liu, Q. A-Site Perovskite Oxides: An Emerging Functional Material for Electrocatalysis and Photocatalysis. *J. Mater. Chem. A* **2021**, *9*, 6650–6670. [CrossRef]
8. Green, M.; Dunlop, E.; Hohl-Ebinger, J.; Yoshita, M.; Kopidakis, N.; Hao, X. Solar Cell Efficiency Tables (Version 57). *Prog. Photovolt. Res. Appl.* **2021**, *29*, 3–15. [CrossRef]
9. Liu, Y.; Li, Z.; Xu, J.; Dong, Y.; Chen, B.; Park, S.M.; Ma, D.; Lee, S.; Huang, J.E.; Teale, S. Wide-Bandgap Perovskite Quantum Dots in Perovskite Matrix for Sky-Blue Light-Emitting Diodes. *J. Am. Chem. Soc.* **2022**, *144*, 4009–4016. [CrossRef]
10. Liu, S.; Biju, V.P.; Qi, Y.; Chen, W.; Liu, Z. Recent Progress in the Development of High-Efficiency Inverted Perovskite Solar Cells. *NPG Asia Mater.* **2023**, *15*, 27. [CrossRef]
11. Suresh Kumar, N.; Chandra Babu Naidu, K. A Review on Perovskite Solar Cells (PSCs), Materials and Applications. *J. Mater.* **2021**, *7*, 940–956. [CrossRef]
12. Li, X.; Zhang, W.; Guo, X.; Lu, C.; Wei, J.; Fang, J. Constructing Heterojunctions by Surface Sulfidation for Efficient Inverted Perovskite Solar Cells. *Science* **2022**, *375*, 434–437. [CrossRef]
13. Chen, H.; Teale, S.; Chen, B.; Hou, Y.; Grater, L.; Zhu, T.; Bertens, K.; Park, S.M.; Atapattu, H.R.; Gao, Y.; et al. Quantum-Size-Tuned Heterostructures Enable Efficient and Stable Inverted Perovskite Solar Cells. *Nat. Photon.* **2022**, *16*, 352–358. [CrossRef]
14. Jeng, J.-Y.; Chiang, Y.-F.; Lee, M.-H.; Peng, S.-R.; Guo, T.-F.; Chen, P.; Wen, T.-C. CH$_3$NH$_3$PbI$_3$ Perovskite/Fullerene Planar-Heterojunction Hybrid Solar Cells. *Adv. Mater.* **2013**, *25*, 3727–3732. [CrossRef] [PubMed]
15. Chen, W.; Wu, Y.; Yue, Y.; Liu, J.; Zhang, W.; Yang, X.; Chen, H.; Bi, E.; Ashraful, I.; Grätzel, M.; et al. Efficient and Stable Large-Area Perovskite Solar Cells with Inorganic Charge Extraction Layers. *Science* **2015**, *350*, 944–948. [CrossRef] [PubMed]
16. Zheng, X.; Hou, Y.; Bao, C.; Yin, J.; Yuan, F.; Huang, Z.; Song, K.; Liu, J.; Troughton, J.; Gasparini, N.; et al. Managing Grains and Interfaces via Ligand Anchoring Enables 22.3%-Efficiency Inverted Perovskite Solar Cells. *Nat. Energy* **2020**, *5*, 131–140. [CrossRef]
17. Li, Z.; Li, B.; Wu, X.; Sheppard, S.A.; Zhang, S.; Gao, D.; Long, N.J.; Zhu, Z. Organometallic-Functionalized Interfaces for Highly Efficient Inverted Perovskite Solar Cells. *Science* **2022**, *376*, 416–420. [CrossRef] [PubMed]
18. Jiang, Q.; Tong, J.; Xian, Y.; Kerner, R.A.; Dunfield, S.P.; Xiao, C.; Scheidt, R.A.; Kuciauskas, D.; Wang, X.; Hautzinger, M.P.; et al. Surface Reaction for Efficient and Stable Inverted Perovskite Solar Cells. *Nature* **2022**, *611*, 278–283. [CrossRef]
19. Babayigit, A.; Ethirajan, A.; Muller, M.; Conings, B. Toxicity of Organometal Halide Perovskite Solar Cells. *Nat. Mater.* **2016**, *15*, 247–251. [CrossRef]
20. Zhao, X.-G.; Yang, D.; Ren, J.-C.; Sun, Y.; Xiao, Z.; Zhang, L. Rational Design of Halide Double Perovskites for Optoelectronic Applications. *Joule* **2018**, *2*, 1662–1673. [CrossRef]
21. Sun, Q.; Wang, J.; Yin, W.-J.; Yan, Y. Bandgap Engineering of Stable Lead-Free Oxide Double Perovskites for Photovoltaics. *Adv. Mater.* **2018**, *30*, 1705901. [CrossRef]
22. R, S.K.; Akande, A.; El-Mellouhi, F.; Park, H.; Sanvito, S. Theoretical Investigation of the Structural, Elastic, Electronic, and Dielectric Properties of Alkali-Metal-Based Bismuth Ternary Chalcogenides. *Phys. Rev. Mater.* **2020**, *4*, 075401. [CrossRef]
23. Obada, D.O.; Abolade, S.A.; R., S.K.; Ukpong, A.M.; Akande, A. Ab Initio Calculations of the Properties of Defective CsSnCl$_3$: The Role of Anion-Cation Pair Defect. *Solid State Ion.* **2023**, *399*, 116262. [CrossRef]

24. Shao, S.; Liu, J.; Portale, G.; Fang, H.-H.; Blake, G.R.; ten Brink, G.H.; Koster, L.J.A.; Loi, M.A. Highly Reproducible Sn-Based Hybrid Perovskite Solar Cells with 9% Efficiency. *Adv. Energy Mater.* **2018**, *8*, 1702019. [CrossRef]

25. Hoefler, S.F.; Trimmel, G.; Rath, T. Progress on Lead-Free Metal Halide Perovskites for Photovoltaic Applications: A Review. *Monatshefte Chem.* **2017**, *148*, 795–826. [CrossRef]

26. Sun, P.-P.; Li, Q.-S.; Yang, L.-N.; Li, Z.-S. Theoretical Insights into a Potential Lead-Free Hybrid Perovskite: Substituting Pb^{2+} with Ge^{2+}. *Nanoscale* **2016**, *8*, 1503–1512. [CrossRef]

27. Subramanian, M.A.; Aravamudan, G.; Rao, G.S. Oxide Pyrochlores—A Review. *Prog. Solid State Chem.* **1983**, *15*, 55–143. [CrossRef]

28. Zhao, X.-G.; Yang, D.; Sun, Y.; Li, T.; Zhang, L.; Yu, L.; Zunger, A. Cu–In Halide Perovskite Solar Absorbers. *J. Am. Chem. Soc.* **2017**, *139*, 6718–6725. [CrossRef]

29. Zhao, X.-G.; Yang, J.-H.; Fu, Y.; Yang, D.; Xu, Q.; Yu, L.; Wei, S.-H.; Zhang, L. Design of Lead-Free Inorganic Halide Perovskites for Solar Cells via Cation-Transmutation. *J. Am. Chem. Soc.* **2017**, *139*, 2630–2638. [CrossRef]

30. Wei, F.; Deng, Z.; Sun, S.; Xie, F.; Kieslich, G.; Evans, D.M.; Carpenter, M.A.; Bristowe, P.D.; Cheetham, A.K. The Synthesis, Structure and Electronic Properties of a Lead-Free Hybrid Inorganic–Organic Double Perovskite $(MA)_2 KBiCl_6$ (MA = Methylammonium). *Mater. Horiz.* **2016**, *3*, 328–332. [CrossRef]

31. Deng, Z.; Wei, F.; Sun, S.; Kieslich, G.; Cheetham, A.K.; Bristowe, P.D. Exploring the Properties of Lead-Free Hybrid Double Perovskites Using a Combined Computational-Experimental Approach. *J. Mater. Chem. A* **2016**, *4*, 12025–12029. [CrossRef]

32. Volonakis, G.; Haghighirad, A.A.; Milot, R.L.; Sio, W.H.; Filip, M.R.; Wenger, B.; Johnston, M.B.; Herz, L.M.; Snaith, H.J.; Giustino, F. $Cs_2InAgCl_6$: A New Lead-Free Halide Double Perovskite with Direct Band Gap. *J. Phys. Chem. Lett.* **2017**, *8*, 772–778. [CrossRef] [PubMed]

33. Tang, T.; Tang, Y. First Principle Comparative Study of Transitional Elements Co, Rh, Ir (III)-Based Double Halide Perovskites. *Mater. Today Commun.* **2023**, *34*, 105431. [CrossRef]

34. Vasala, S.; Karppinen, M. $A_2B'B''O_6$ Perovskites: A Review. *Prog. Solid State Chem.* **2015**, *43*, 1–36. [CrossRef]

35. Hossain, A.; Bandyopadhyay, P.; Roy, S. An Overview of Double Perovskites $A_2B'B''O_6$ with Small Ions at A Site: Synthesis, Structure and Magnetic Properties. *J. Alloys Compd.* **2018**, *740*, 414–427. [CrossRef]

36. Tian, J.; Xue, Q.; Yao, Q.; Li, N.; Brabec, C.J.; Yip, H.-L. Inorganic Halide Perovskite Solar Cells: Progress and Challenges. *Adv. Energy Mater.* **2020**, *10*, 2000183. [CrossRef]

37. Gao, Y.; Pan, Y.; Zhou, F.; Niu, G.; Yan, C. Lead-Free Halide Perovskites: A Review of the Structure–Property Relationship and Applications in Light Emitting Devices and Radiation Detectors. *J. Mater. Chem. A* **2021**, *9*, 11931–11943. [CrossRef]

38. Travis, W.; Glover, E.N.K.; Bronstein, H.; Scanlon, D.O.; Palgrave, R.G. On the Application of the Tolerance Factor to Inorganic and Hybrid Halide Perovskites: A Revised System. *Chem. Sci.* **2016**, *7*, 4548–4556. [CrossRef]

39. Li, C.; Lu, X.; Ding, W.; Feng, L.; Gao, Y.; Guo, Z. Formability of ABX_3 (X = F, Cl, Br, I) Halide Perovskites. *Acta Crystallogr. Sect. B* **2008**, *64*, 702–707. [CrossRef]

40. Xiao, Z.; Yan, Y. Progress in Theoretical Study of Metal Halide Perovskite Solar Cell Materials. *Adv. Energy Mater.* **2017**, *7*, 1701136. [CrossRef]

41. Yin, H.; Xian, Y.; Zhang, Y.; Li, W.; Fan, J. Structurally Stabilizing and Environment Friendly Triggers: Double-Metallic Lead-Free Perovskites. *Solar RRL* **2019**, *3*, 1900148. [CrossRef]

42. Wu, Y.; Li, X.; Zeng, H. Lead-Free Halide Double Perovskites: Structure, Luminescence, and Applications. *Small Struct.* **2021**, *2*, 2000071. [CrossRef]

43. Mahmood, Q.; Ghrib, T.; Rached, A.; Laref, A.; Kamran, M.A. Probing of Mechanical, Optical and Thermoelectric Characteristics of Double Perovskites Cs_2GeCl/Br_6 by DFT Method. *Mater. Sci. Semicond. Process.* **2020**, *112*, 105009. [CrossRef]

44. Iqbal, S.; Mustafa, G.M.; Asghar, M.; Noor, N.A.; Iqbal, M.W.; Mahmood, A.; Shin, Y.-H. Tuning the Optoelectronic and Thermoelectric Characteristics of Narrow Bandgap Rb_2AlInX_6(X= Cl, Br, I) Double Perovskites: A DFT Study. *Mater. Sci. Semicond. Process.* **2022**, *143*, 106551. [CrossRef]

45. Mahmood, Q.; Younas, M.; Ashiq, M.G.B.; Ramay, S.M.; Mahmood, A.; Ghaithan, H.M. First Principle Study of Lead-Free Double Perovskites Halides $Rb_2Pd(Cl/Br)_6$ for Solar Cells and Renewable Energy Devices: A Quantum DFT. *Int. J. Energy Res.* **2021**, *45*, 14995–15004. [CrossRef]

46. Kibbou, M.; Haman, Z.; Bouziani, I.; Khossossi, N.; Benhouria, Y.; Essaoudi, I.; Ainane, A.; Ahuja, R. Cs_2InGaX_6 (X=Cl, Br, or I): Emergent Inorganic Halide Double Perovskites with Enhanced Optoelectronic Characteristics. *Curr. Appl. Phys.* **2021**, *21*, 50–57. [CrossRef]

47. Noor, N.A.; Iqbal, M.W.; Zelai, T.; Mahmood, A.; Shaikh, H.M.; Ramay, S.M.; Al-Masry, W. Analysis of Direct Band Gap A_2ScInI_6 (A=Rb, Cs) Double Perovskite Halides Using DFT Approach for Renewable Energy Devices. *J. Mater. Res. Technol.* **2021**, *13*, 2491–2500. [CrossRef]

48. Chrafih, Y.; Al-Hattab, M.; Rahmani, K. Thermodynamic, Optical, and Morphological Studies of the Cs_2AgBiX_6 Double Perovskites (X = Cl, Br, and I): Insights from DFT Study. *J. Alloys Compd.* **2023**, *960*, 170650. [CrossRef]

49. Rajeev Kumar, N.; Radhakrishnan, R. Electronic, Optical and Mechanical Properties of Lead-Free Halide Double Perovskites Using First-Principles Density Functional Theory. *Mater. Lett.* **2018**, *227*, 289–291. [CrossRef]

50. Iqbal, M.W.; Manzoor, M.; Gouadria, S.; Asghar, M.; Zainab, M.; Ahamd, N.N.; Aftab, S.; Sharma, R.; Zahid, T. DFT Insights on the Opto-Electronic and Thermoelectric Properties of Double Perovskites K_2AgSbX_6 (X = Cl, Br) via Halides Substitutions for Solar Cell Applications. *Mater. Sci. Eng. B* **2023**, *290*, 116338. [CrossRef]

51. Talebi, M.; Mokhtari, A.; Soleimanian, V. Ab-Inito Simulation of the Structural, Electronic and Optical Properties for the Vacancy-Ordered Double Perovskites A_2TiI_6 (A = Cs or NH_4); a Time-Dependent Density Functional Theory Study. *J. Phys. Chem. Solids* **2023**, *176*, 111262. [CrossRef]

52. Ud Din, M.; Munir, J.; Jamil, M.; Saeed, M.A.; Ain, Q. Electronic Structure and Optical Response of Double Perovskite Rb_2NaCoF_6 for Optoelectronic Devices. *Phys. B Condens. Matter* **2022**, *627*, 413533. [CrossRef]

53. VanOrman, Z.A.; Nienhaus, L. Recent Advancements in Halide Perovskite Nanomaterials and Their Optoelectronic Applications. *InfoMat* **2021**, *3*, 962–986. [CrossRef]

54. Menedjhi, A.; Bouarissa, N.; Saib, S.; Boucenna, M.; Mezrag, F. Band Structure and Optical Spectra of Double Perovskite $Cs_2AgBiBr_6$ for Solar Cells Performance. *Acta Phys. Pol. A* **2020**, *137*, 486. [CrossRef]

55. Sun, Q.; Yin, W.-J.; Wei, S.-H. Searching for Stable Perovskite Solar Cell Materials Using Materials Genome Techniques and High-Throughput Calculations. *J. Mater. Chem. C* **2020**, *8*, 12012–12035. [CrossRef]

56. Slavney, A.H.; Hu, T.; Lindenberg, A.M.; Karunadasa, H.I. A Bismuth-Halide Double Perovskite with Long Carrier Recombination Lifetime for Photovoltaic Applications. *J. Am. Chem. Soc.* **2016**, *138*, 2138–2141. [CrossRef] [PubMed]

57. Filip, M.R.; Hillman, S.; Haghighirad, A.A.; Snaith, H.J.; Giustino, F. Band Gaps of the Lead-Free Halide Double Perovskites $Cs_2BiAgCl_6$ and $Cs_2BiAgBr_6$ from Theory and Experiment. *J. Phys. Chem. Lett.* **2016**, *7*, 2579–2585. [CrossRef] [PubMed]

58. Yang, J.; Zhang, P.; Wei, S.-H. Band Structure Engineering of $Cs_2AgBiBr_6$ Perovskite through Order–Disordered Transition: A First-Principle Study. *J. Phys. Chem. Lett.* **2018**, *9*, 31–35. [CrossRef]

59. Liang, L.; Gao, P. Lead-Free Hybrid Perovskite Absorbers for Viable Application: Can We Eat the Cake and Have It Too? *Adv. Sci.* **2018**, *5*, 1700331. [CrossRef]

60. McClure, E.T.; Ball, M.R.; Windl, W.; Woodward, P.M. Cs_2AgBiX_6 (X = Br, Cl): New Visible Light Absorbing, Lead-Free Halide Perovskite Semiconductors. *Chem. Mater.* **2016**, *28*, 1348–1354. [CrossRef]

61. Hoye, R.L.Z.; Schulz, P.; Schelhas, L.T.; Holder, A.M.; Stone, K.H.; Perkins, J.D.; Vigil-Fowler, D.; Siol, S.; Scanlon, D.O.; Zakutayev, A.; et al. Perovskite-Inspired Photovoltaic Materials: Toward Best Practices in Materials Characterization and Calculations. *Chem. Mater.* **2017**, *29*, 1964–1988. [CrossRef]

62. Volonakis, G.; Filip, M.R.; Haghighirad, A.A.; Sakai, N.; Wenger, B.; Snaith, H.J.; Giustino, F. Lead-Free Halide Double Perovskites via Heterovalent Substitution of Noble Metals. *J. Phys. Chem. Lett.* **2016**, *7*, 1254–1259. [CrossRef]

63. Haug, H.; Koch, S.W. *Quantum Theory of the Optical and Electronic Properties of Semiconductors*; World Scientific Publishing Company: Singapore, 2009; Volume 10, p. 7184.

64. Gao, Y.; Wang, X.; Mi, W. Tunable Electronic Structure and Magnetic Properties of Two-Dimensional $g\text{-}C_3N_4/Cr_2Ge_2Te_6$ van Der Waals Heterostructures. *Comput. Mater. Sci.* **2021**, *187*, 110085. [CrossRef]

65. Komsa, H.-P.; Krasheninnikov, A.V. Native Defects in Bulk and Monolayer MoS_2 from First Principles. *Phys. Rev. B* **2015**, *91*, 125304. [CrossRef]

66. Maqsood, S.; Murtaza, G.; Noor, N.A.; Neffati, R.; Nazir, S.; Laref, A. First-Principle Investigation of Thermoelectric and Optoelectronic Properties of Rb_2KScI_6 and Cs_2KScI_6 Double Perovskite for Solar Cell Devices. *J. Mater. Res. Technol.* **2022**, *21*, 841–849. [CrossRef]

67. Radja, K.; Farah, B.L.; Ibrahim, A.; Lamia, D.; Fatima, I.; Nabil, B.; Mohamed, A.; Al-Douri, Y.; Abd El-Rehim, A.F. Investigation of Structural, Magneto-Electronic, Elastic, Mechanical and Thermoelectric Properties of Novel Lead-Free Halide Double Perovskite $Cs_2AgFeCl_6$: First-Principles Calcuations. *J. Phys. Chem. Solids* **2022**, *167*, 110795. [CrossRef]

68. Aldaghfag, S.A.; Aziz, A.; Younas, A.; Yaseen, M.; Murtaza, A.; Hegazy, H.H. Investigation of Electronic, Optical and Thermoelectric Features of $X_2ScAgCl_6$ (X=K, Na) Double Perovskites for Renewable Energy Applications. *J. Solid State Chem.* **2022**, *312*, 123179. [CrossRef]

69. Kattan, N.A.; Rouf, S.A.; Sfina, N.; mana Al-Anazy, M.; Ullah, H.; Hakamy, A.; Mera, A.; Mahmood, Q.; Amin, M.A. Tuning of Band Gap by Anion Variation of Double Perovskites K_2AgInX_6 (X=Cl, Br) for Solar Cells and Thermoelectric Applications. *J. Solid State Chem.* **2023**, *319*, 123820. [CrossRef]

70. Shah, S.Z.A.; Niaz, S. Lead-Free Indium-Silver Based Double Perovskites for Thermoelectric Applications: Structural, Electronic and Thermoelectric Properties Using First-Principles Approach. *Mater. Today Commun.* **2021**, *28*, 102609. [CrossRef]

71. Aslam, F.; Ullah, H.; Hassan, M. Theoretical Investigation of Cs_2InBiX_6 (X=Cl, Br, I) Double Perovskite Halides Using First-Principle Calculations. *Mater. Sci. Eng. B* **2021**, *274*, 115456. [CrossRef]

72. Al-Qaisi, S.; Mushtaq, M.; Alomairy, S.; Vu, T.V.; Rached, H.; Haq, B.U.; Mahmood, Q.; Al-Buriahi, M.S. First-Principles Investigations of Na_2CuMCl_6 (M= Bi, Sb) Double Perovskite Semiconductors: Materials for Green Technology. *Mater. Sci. Semicond. Process.* **2022**, *150*, 106947. [CrossRef]

73. Hu, D.-Y.; Zhao, X.-H.; Tang, T.-Y.; Lu, L.-M.; Li, L.; Gao, L.-K.; Tang, Y.-L. Revealing Structural, Elastic, Electronic and Optical Properties of Potential Perovskites K_2CuBiX_6 (X=Br, Cl) Based on First-Principles. *J. Solid State Chem.* **2022**, *310*, 123046. [CrossRef]

74. Zhao, S.; Yamamoto, K.; Iikubo, S.; Hayase, S.; Ma, T. First-Principles Study of Electronic and Optical Properties of Lead-Free Double Perovskites Cs_2NaBX_6 (B = Sb, Bi; X=Cl, Br, I). *J. Phys. Chem. Solids* **2018**, *117*, 117–121. [CrossRef]

75. Manzoor, M.; Iqbal, M.W.; Noor, N.A.; Ullah, H.; Sharma, R.; Alarfaji, S.S. Exploring the Structural, Electronic, Optical, and Thermoelectric Properties of Potassium-Based Double Perovskites K_2AgXI_6 (X=Sb, Bi) Compounds: A DFT Study. *Mater. Sci. Eng. B* **2023**, *287*, 116122. [CrossRef]

76. Murtaza, G.; Alshahrani, T.; Khalil, R.A.; Mahmood, Q.; Flemban, T.H.; Althib, H.; Laref, A. Lead Free Double Perovsites Halides $X_2AgTlCl_6$ (X=Rb, Cs) for Solar Cells and Renewable Energy Applications. *J. Solid State Chem.* **2021**, *297*, 121988. [CrossRef]

77. Maiti, T.; Saxena, M.; Roy, P. Double Perovskite (Sr2B′B″O6) Oxides for High-Temperature Thermoelectric Power Generation—A Review. *J. Mater. Res.* **2019**, *34*, 107–125. [CrossRef]

78. Bhandari, S.R.; Yadav, D.K.; Belbase, B.P.; Zeeshan, M.; Sadhukhan, B.; Rai, D.P.; Thapa, R.K.; Kaphle, G.C.; Ghimire, M.P. Electronic, Magnetic, Optical and Thermoelectric Properties of $Ca_2Cr_{1−x}NixOsO_6$ Double Perovskites. *RSC Adv.* **2020**, *10*, 16179–16186. [CrossRef] [PubMed]

79. Albalawi, H.; Mustafa, G.M.; Saba, S.; Kattan, N.A.; Mahmood, Q.; Somaily, H.H.; Morsi, M.; Alharthi, S.; Amin, M.A. Study of Optical and Thermoelectric Properties of Double Perovskites Cs_2KTlX_6 (X = Cl, Br, I) for Solar Cell and Energy Harvesting. *Mater. Today Commun.* **2022**, *32*, 104083. [CrossRef]

80. Flemban, T.H.; Zelai, T.; Mahmood, Q.; Devi, A.A.S.; Sajjad, M.; Alhossainy, M.H.; Somaily, H.H.; Mera, A.; Alharthi, S.; Amin, M.A. Half-Metallic Ferromagnetism and Thermoelectric Properties of Double Perovskites Rb2Z(Cl/Br)6 (Z = Ta, W, Re). *J. Alloys Compd.* **2022**, *894*, 162313. [CrossRef]

81. Khandy, S.A.; Gupta, D.C. Electronic Structure, Magnetism and Thermoelectric Properties of Double Perovskite Sr_2HoNbO_6. *J. Magn. Magn. Mater.* **2018**, *458*, 176–182. [CrossRef]

82. Saxena, M.; Maiti, T. Effect of Ba-Doping on High Temperature Thermoelectric Properties of Sr_2TiMoO_6 Double Perovskites. *J. Alloys Compd.* **2017**, *710*, 472–478. [CrossRef]

83. Sudha; Saxena, M.; Balani, K.; Maiti, T. Structure and Thermoelectric Properties of Calcium Doped Sr_2TiCoO_6 Double Perovskites. *Mater. Sci. Eng. B* **2019**, *244*, 65–71. [CrossRef]

84. Guechi, N.; Bouhemadou, A.; Bin-Omran, S.; Bourzami, A.; Louail, L. Elastic, Optoelectronic and Thermoelectric Properties of the Lead-Free Halide Semiconductors Cs_2AgBiX_6 (X=Cl, Br): Ab Initio Investigation. *J. Electron. Mater.* **2018**, *47*, 1533–1545. [CrossRef]

85. Senkov, O.N.; Miracle, D.B. Generalization of Intrinsic Ductile-to-Brittle Criteria by Pugh and Pettifor for Materials with a Cubic Crystal Structure. *Sci. Rep.* **2021**, *11*, 4531. [CrossRef]

86. Greaves, G.N.; Greer, A.L.; Lakes, R.S.; Rouxel, T. Poisson's Ratio and Modern Materials. *Nat. Mater.* **2011**, *10*, 823–837. [CrossRef] [PubMed]

87. Anbarasan, R.; Balasubramani, V.; Srinivasan, M.; Sundar, J.K.; Ramasamy, P.; Al-Kahtani, A.A.; Ubaidullah, M.; Setiawan, I.A.; Kim, W.K.; Gedi, S. First Principle Insights on Mechanical, Electronic and Optical Properties of Direct Bandgap Material Cs_2KScX_6 (X=Cl, Br and I) for Optoelectronic Applications. *J. Solid State Chem.* **2022**, *316*, 123590. [CrossRef]

88. Gubernatis, J.E.; Lookman, T. Machine Learning in Materials Design and Discovery: Examples from the Present and Suggestions for the Future. *Phys. Rev. Mater.* **2018**, *2*, 120301. [CrossRef]

89. Jacobs, R.; Luo, G.; Morgan, D. Materials Discovery of Stable and Nontoxic Halide Perovskite Materials for High-Efficiency Solar Cells. *Adv. Funct. Mater.* **2019**, *29*, 1804354. [CrossRef]

90. Allam, O.; Holmes, C.; Greenberg, Z.; Kim, K.C.; Jang, S.S. Density Functional Theory—Machine Learning Approach to Analyze the Bandgap of Elemental Halide Perovskites and Ruddlesden-Popper Phases. *ChemPhysChem* **2018**, *19*, 2559–2565. [CrossRef] [PubMed]

91. Liu, Y.; Wu, J.; Wang, Z.; Lu, X.-G.; Avdeev, M.; Shi, S.; Wang, C.; Yu, T. Predicting Creep Rupture Life of Ni-Based Single Crystal Superalloys Using Divide-and-Conquer Approach Based Machine Learning. *Acta Mater.* **2020**, *195*, 454–467. [CrossRef]

92. Pilania, G.; Mannodi-Kanakkithodi, A.; Uberuaga, B.P.; Ramprasad, R.; Gubernatis, J.E.; Lookman, T. Machine Learning Bandgaps of Double Perovskites. *Sci. Rep.* **2016**, *6*, 19375. [CrossRef] [PubMed]

93. Ramprasad, R.; Batra, R.; Pilania, G.; Mannodi-Kanakkithodi, A.; Kim, C. Machine Learning in Materials Informatics: Recent Applications and Prospects. *NPJ Comput. Mater.* **2017**, *3*, 54. [CrossRef]

94. Himanen, L.; Geurts, A.; Foster, A.S.; Rinke, P. Data-Driven Materials Science: Status, Challenges, and Perspectives. *Adv. Sci.* **2019**, *6*, 1900808. [CrossRef]

95. Sun, J.-P.; McKeown Wessler, G.C.; Wang, T.; Zhu, T.; Blum, V.; Mitzi, D.B. Structural Tolerance Factor Approach to Defect-Resistant I2-II-IV-X4 Semiconductor Design. *Chem. Mater.* **2020**, *32*, 1636–1649. [CrossRef]

96. Wan, X.; Feng, W.; Wang, Y.; Wang, H.; Zhang, X.; Deng, C.; Yang, N. Materials Discovery and Properties Prediction in Thermal Transport via Materials Informatics: A Mini Review. *Nano Lett.* **2019**, *19*, 3387–3395. [CrossRef] [PubMed]

97. Shafizadeh, A.; Shahbeig, H.; Nadian, M.H.; Mobli, H.; Dowlati, M.; Gupta, V.K.; Peng, W.; Lam, S.S.; Tabatabaei, M.; Aghbashlo, M. Machine Learning Predicts and Optimizes Hydrothermal Liquefaction of Biomass. *Chem. Eng. J.* **2022**, *445*, 136579. [CrossRef]

98. Toyao, T.; Maeno, Z.; Takakusagi, S.; Kamachi, T.; Takigawa, I.; Shimizu, K. Machine Learning for Catalysis Informatics: Recent Applications and Prospects. *ACS Catal.* **2020**, *10*, 2260–2297. [CrossRef]

99. Chen, C.; Zuo, Y.; Ye, W.; Li, X.; Deng, Z.; Ong, S.P. A Critical Review of Machine Learning of Energy Materials. *Adv. Energy Mater.* **2020**, *10*, 1903242. [CrossRef]

100. Zhou, T.; Song, Z.; Sundmacher, K. Big Data Creates New Opportunities for Materials Research: A Review on Methods and Applications of Machine Learning for Materials Design. *Engineering* **2019**, *5*, 1017–1026. [CrossRef]

101. Shi, L.; Chang, D.; Ji, X.; Lu, W. Using Data Mining To Search for Perovskite Materials with Higher Specific Surface Area. *J. Chem. Inf. Model.* **2018**, *58*, 2420–2427. [CrossRef] [PubMed]

102. Tao, Q.; Xu, P.; Li, M.; Lu, W. Machine Learning for Perovskite Materials Design and Discovery. *NPJ Comput. Mater.* **2021**, *7*, 23. [CrossRef]

103. Talapatra, A.; Uberuaga, B.P.; Stanek, C.R.; Pilania, G. Band Gap Predictions of Double Perovskite Oxides Using Machine Learning. *Commun. Mater.* **2023**, *4*, 46. [CrossRef]

104. Zhang, J.; Li, Y.; Zhou, X. Machine-Learning Prediction of the Computed Band Gaps of Double Perovskite Materials. *arXiv* **2023**, arXiv:2301.03372.

105. Obada, D.O.; Okafor, E.; Abolade, S.A.; Ukpong, A.M.; Dodoo-Arhin, D.; Akande, A. Explainable Machine Learning for Predicting the Band Gaps of ABX_3 Perovskites. *Mater. Sci. Semicond. Process.* **2023**, *161*, 107427. [CrossRef]

106. Kirklin, S.; Saal, J.E.; Meredig, B.; Thompson, A.; Doak, J.W.; Aykol, M.; Rühl, S.; Wolverton, C. The Open Quantum Materials Database (OQMD): Assessing the Accuracy of DFT Formation Energies. *NPJ Comput. Mater.* **2015**, *1*, 15010. [CrossRef]

107. Jain, A.; Ong, S.P.; Hautier, G.; Chen, W.; Richards, W.D.; Dacek, S.; Cholia, S.; Gunter, D.; Skinner, D.; Ceder, G. Commentary: The Materials Project: A Materials Genome Approach to Accelerating Materials Innovation. *APL Mater.* **2013**, *1*, 011002. [CrossRef]

108. Landis, D.D.; Hummelshøj, J.S.; Nestorov, S.; Greeley, J.; Dułak, M.; Bligaard, T.; Nørskov, J.K.; Jacobsen, K.W. The Computational Materials Repository. *Comput. Sci. Eng.* **2012**, *14*, 51–57. [CrossRef]

109. Curtarolo, S. Using Your Own Computer to Search for Novel Materials (with a Little Help from the Aflowlib. Org Consortium Online Library). *Bull. Am. Phys. Soc.* **2014**, *59*, 273.

110. Curtarolo, S.; Setyawan, W.; Wang, S.; Xue, J.; Yang, K.; Taylor, R.H.; Nelson, L.J.; Hart, G.L.; Sanvito, S.; Buongiorno-Nardelli, M. AFLOWLIB. ORG: A Distributed Materials Properties Repository from High-Throughput Ab Initio Calculations. *Comput. Mater. Sci.* **2012**, *58*, 227–235. [CrossRef]